Space Sci Rev (2008) 139: 107–141
DOI 10.1007/s11214-008-9401-9

Neutral Upper Atmosphere and Ionosphere Modeling

Stephen W. Bougher · Pierre-Louis Blelly · Michael Combi · Jane L. Fox · Ingo Mueller-Wodarg · Aaron Ridley · Raymond G. Roble

Received: 29 February 2008 / Accepted: 9 June 2008 / Published online: 15 July 2008

Abstract Numerical modeling tools can be used for a number of reasons yielding many benefits in their application to planetary upper atmosphere and ionosphere environments. These tools are commonly used to predict upper atmosphere and ionosphere characteristics and to interpret measurements once they are obtained. Additional applications of these tools include conducting diagnostic balance studies, converting raw measurements into useful physical parameters, and comparing features and processes of different planetary atmospheres. This chapter focuses upon various classes of upper atmosphere and ionosphere numerical modeling tools, the equations solved and key assumptions made, specified inputs and tunable parameters, their common applications, and finally their notable strengths and weaknesses. Examples of these model classes and their specific applications to individual planetary environments will be described.

Keywords Planets · Thermospheres · Ionospheres · Numerical modeling

S.W. Bougher (✉) · M. Combi · A. Ridley
Atmospheric, Oceanic and Space Sciences Department, University of Michigan, Ann Arbor, MI 48109-2143, USA
e-mail: bougher@umich.edu

P.-L. Blelly
CESR, Toulouse, France

J.L. Fox
Wright State University, Dayton, OH 45435, USA

I. Mueller-Wodarg
Imperial College London, London, UK

R.G. Roble
National Center for Atmospheric Research, Boulder, CO 80309, USA

1 Introduction and Scope

The arrival of new measurements of the neutral upper atmospheres and ionospheres of various solar system planets and moons over the past 4-decades from various spacecraft missions has been astounding (e.g., see Mueller-Wodarg et al. 2008; Witasse et al. 2008; Johnson et al. 2008, and other chapters from this book). These measurements have been used to characterize the structure and dynamics of these atmospheric environments and to compare them to one another. A corresponding evolution of modeling tools, from simple to complex frameworks, has occurred over the same timeframe. These tools are commonly used to predict upper atmosphere and ionosphere characteristics and to interpret measurements once they are obtained. This chapter focuses upon various classes of upper atmosphere and ionosphere numerical modeling tools, the equations solved and assumptions, specified inputs and tunable parameters, their applications, and finally their notable strengths and weaknesses. Examples of these model classes and their specific applications to individual planetary environments will be described.

1.1 General Uses/Benefits of Modeling Tools

Numerical modeling tools can be used for a number of reasons yielding many benefits in their application to planetary upper atmosphere and ionosphere environments. First and foremost, modeling tools are commonly utilized to understand the processes that maintain observed atmospheric structures and drive their variations over various timescales (e.g., solar cycle, seasonal, diurnal, etc.). Time varying inputs (e.g., solar) are often specified to drive model simulations and monitor the resulting variations among the simulated fields. These same model simulations can also be examined to provide a diagnostic analysis of the individual terms of the solved equations; e.g. thermal and momentum balances. Such diagnostic studies provide valuable insight into the underlying processes that are responsible for the time variable features of the atmosphere. Spatially or temporally limited measurements are commonly used to constrain model simulations in an effort to construct reasonable predictions outside available dataset domains and/or time periods. This effort places available observations in a more general/global context. Such model predictions can also be used to motivate new measurements and/or conduct more thorough data analysis studies combining existing datasets.

Model simulations can also be utilized in data processing to facilitate the conversion of raw measurements into useful physical parameters. A good example involves the analysis of aerobraking accelerometer measurements (e.g. Withers 2006; Tolson et al. 2007). Raw accelerations are typically calibrated to yield mass densities and corresponding scale heights. The estimation of temperatures from these density scale heights requires independent information about the composition of the thermosphere (e.g. relative abundance of atomic and molecular species). Global thermospheric general circulation model (TGCM) simulations for Mars are available to provide a first estimate of these global abundances, enabling neutral temperatures to be estimated from scale heights (see Sect. 4.2.5 below).

The comparative approach to investigating planetary upper atmospheres is becoming increasingly fruitful as new information from various planet atmospheres is assimilated using state-of-the-art modeling tools (e.g., Bougher et al. 2002). A comparison of the basic features of the structure and dynamics of planetary upper atmospheres and ionospheres can often be understood by examining the implications of their fundamental planetary parameters (e.g., Bougher et al. 1999a, 2000, 2002; Rishbeth et al. 2000b). Such analysis can be used to guide new model simulations (e.g., to estimate the relative importance of individual

processes), and to subsequently interpret completed model simulations. Recent studies have also shown that substantial advances in our understanding can be realized by investigating common aeronomic processes across various planetary environments. A common modeling framework, modified to incorporate planet specific fundamental parameters, provides a useful platform for examining the relative importance of these common physical processes. Finally, model predictions for planetary upper atmospheres and ionospheres with limited or no measurements are often made based upon our experience with previously successful model frameworks encompassing similar physical processes (see Sect. 1.2).

1.2 Usefulness and Shortcomings of the Earth Paradigm

Terrestrial modeling frameworks and their assumptions have typically been used to launch new simulations of other planetary upper atmospheres and ionospheres. This terrestrial paradigm is both useful and hazardous at the same time. The primary benefit of the Earth paradigm can be realized for planetary upper atmospheres having similarities in their fundamental planetary parameters, basic processes, and vertical domains (atmospheric regions). Simulations across these similar planetary environments can be effectively used to examine the relative importance of common aeronomic processes. A good example is the determination of the relative importance of CO_2 15-micron emission as a cooling agent in the thermospheres of Venus, Earth, and Mars (e.g., Bougher et al. 1999a, 2000, 2002). However, planet specific assumptions are often applied when casting the model equations to be solved and the physical formulations employed. Furthermore, fundamental planetary parameters may be so different that application of a terrestrial model framework may no longer be appropriate. A good example of the latter is the application of traditional Earth thermospheric models to the upper atmosphere of Saturn's moon Titan (see Sect. 4.2.3). Here, the assumption of constant gravity over the Titan thermospheric domain (~600–1500 km) is not sufficient to characterize the extended atmosphere associated with this small body.

In short, care must be taken when applying an existing modeling framework to a new planetary environment. A review of the key equations to be solved and all supporting assumptions must be made in light of the important processes to be incorporated and the vertical domain to be addressed (see Sect. 2).

1.3 Roadmap for Chapter

This chapter describes various numerical model classes (and representative model tools) that are typically used in simulations of the upper atmospheres and ionospheres of planets. Assumptions about the model equations to be solved by the different model frameworks can be classified by the number of moments carried in the solution of the Boltzmann equation (see Table 1 and Sect. 2). Both 1D and multi-dimensional model frameworks are employed, both for the upper atmosphere (UATM) and whole atmosphere (WATM) environment (see Table 1). One-dimensional models (see Sect. 3) are commonly used to thoroughly test detailed aeronomic processes (e.g., thermal, diffusion, and chemical) before the addition of global winds in a multi-dimensional model framework (see Sect. 4). This progression from 1D to multi-dimensional models follows a development strategy involving increasing complexity, internal self-consistency, and expanded temporal plus spatial coverage. Finally, modeling frontiers and key problems for further research are described in Sect. 5.

Table 1 Classes and Examples of Upper Atmosphere Modeling Tools

Dimensions	5-Moment	8-Moment	13-Moment
1D (UATM)	Earth (Roble)	Earth GITM	Mars
	Venus (Fox)	Mars GITM	
	Mars (Fox)	Titan GITM	
3D (UATM)	Earth TIE-GCM	Earth GITM	
	Earth TIME-GCM	Mars GITM	
	Earth CTIM,CTIP, CMAT	Titan GITM	
	Venus TGCM		
	Mars TGCM		
	Jupiter JIM		
	Jupiter TGCM		
	Saturn STIM		
	Titan TTIM		
3D (WATM)	Earth WACCM	Mars GITM (MWACM)	
	Mars MGCM-MTGCM		
	Mars LMD-MGCM		

TGCM (Thermosphere General Circulation Model); GITM (Global Ionosphere Thermosphere Model); WACCM (Whole Atmosphere Community Climate Model); TIE-GCM (Thermosphere Ionosphere Electrodynamics General Circulation Model); TIME-GCM (Thermosphere Ionosphere Mesosphere Electrodynamics General Circulation Model); CTIM (Coupled Thermosphere Ionosphere Model); CTIP (Coupled Thermosphere Ionosphere Plasmasphere Model); CMAT (Coupled Middle Atmosphere Thermosphere Model); JIM (Jupiter Ionosphere Model); STIM (Saturn Thermosphere Ionosphere Model); TTIM (Titan Thermosphere Ionosphere Model); MWACM (Mars Whole Atmosphere Climate Model); MGCM-MTGCM (Mars General Circulation Model – Mars Thermosphere General Circulation Model); LMD-MGCM (Laboratoire de Meteorologie Dynamique Mars General Circulation Model)

2 Moment Solutions of the Boltzman Equation: Applicability Concerns for Upper Atmosphere Models

There are numerous different ways to obtain the transport equations needed to model neutral atmosphere and ionospheric behavior. The one which starts from basic physical principles uses the so called moments of the Boltzmann equation. In the Boltzmann approach one is not interested in the behavior of individual gas particles, but the gas is described by the velocity distribution function $f_s(\mathbf{r}, \mathbf{v}, t)$, where the subscript s, denotes a given species, s, $\mathbf{r}_s$ is the spatial location, $\mathbf{v}_s$ is the velocity and t is time. It can be easily shown (e.g., Schunk and Nagy 2000) that the integro-differential equation for f_s is:

$$\frac{\partial f_s}{\partial t} + \mathbf{v}_s . \nabla f_s + \mathbf{a}_s . \nabla_v f_s = \frac{\delta f_s}{\delta t} \tag{1}$$

where ∇_s is the velocity gradient and $\delta f_s / \delta t$ is a short hand way to write the change in f_s due to collisions. In order to deduce the transport equations of macroscopic parameters one first defines velocity moments of this distribution function. The most commonly used macroscopic parameters of interest are:

$$n_s(r, t) = \int_{-\infty}^{\infty} d^3 v_s f_s, \tag{2}$$

$$\mathbf{u}_s(\mathbf{r},t) = \int_{-\infty}^{\infty} d^3 v_s f_s \mathbf{v}_s / n_s, \tag{3}$$

$$T_s = \frac{m_s}{3kn_s} d^3 v_s f_s (\mathbf{v}_s - \mathbf{u}_s)^2, \tag{4}$$

$$\mathbf{q}_s = \frac{m_s}{2} \int_{-\infty}^{\infty} d^3 v_s f_s (\mathbf{v}_s - \mathbf{u}_s)^2 (\mathbf{v}_s - \mathbf{u}_s), \tag{5}$$

$$p_s = \frac{m_s}{3} \int_{-\infty}^{\infty} d^3 v_s f_s (\mathbf{v}_s - \mathbf{u}_s)^2, \tag{6}$$

$$\mathbf{P}_s = m_s \int_{-\infty}^{\infty} d^3 v_s f_s (\mathbf{v}_s - \mathbf{u}_s)(\mathbf{v}_s - \mathbf{u}_s), \tag{7}$$

$$\tau_s = \mathbf{P}_s - p_s \mathbf{I}, \tag{8}$$

where n_s is the number density of species s, $\mathbf{u}_s$ is the drift (mean) velocity, T_s is the temperature, $\mathbf{q}_s$ is the heat flow vector, p_s is the scalar pressure, $\mathbf{P}_s$ is the pressure tensor and τ_s is the stress tensor.

In order to obtain the appropriate transport equations for these macroscopic parameters of interest one multiplies the Boltzmann equation with the appropriate function of velocity and then integrates over all velocities. Now a very important point should be noted that the resulting, so called "transport equations", do not lead to a closed system of equations. Namely an equation governing the moment of order k contains the moment of order $(k+1)$. As an example the equation for density contains the drift velocity. A number of approaches have been suggested in order to achieve closure. The most commonly used method finds an approximate expression for the distribution function which allows closure and the evaluation of the collision term.

The so-called 13 moment approximation is the most complex set of equations that have been used so far in neutral atmosphere and ionosphere modeling. In this approach, f_s is approximated as a truncated expansion about the Maxwell Boltzmann distribution function in terms of density, drift velocity, temperature, stress tensor and heat flow vector. The name 13-moment approximation comes from the fact that the gas is described in terms of 13 parameters ($n_s = 1, \mathbf{u}_s = 3, T_s = 1, \mathbf{q}_s = 3, \tau_s = 5$). In most cases the 13 moment equations (see Schunk and Nagy 2000) are too complicated to be able to be solved in a comprehensive global model. The 8-moment equation neglects the stress tensor and the 5 moment equations neglect both stress and heat flow. The Navier-Stokes equation are obtained from the 13-moment equations by assuming that the collision frequency is very high and dropping all $\mathbf{q}_s$ and $\boldsymbol{\tau}_s$ terms, except those that are multiplied by the collision frequency. In this approximation $\mathbf{q}_s$ and $\boldsymbol{\tau}_s$ can be expressed in term of n_s, $\mathbf{u}_s$ and T_s. The most common set of equations used in global models are these Navier-Stokes ones. However, it should be remembered that in this approximation the distribution function must be close to a Maxwellian.

3 Representative 1-D Neutral and/or Ion Models

3.1 Earth

A global mean model of a planetary atmosphere is useful for the development of a self-consistent aeronomical scheme, determining the vertical resolution necessary to determine the basic atmospheric and ionospheric structure, time constants of physical and chemical

processes and a host of other properties of the atmosphere and ionosphere. Such a model is numerically fast for long-time integrations, and easy to test and analyze the sensitivity of the atmosphere to physical and chemical processes, such as eddy diffusion, chemical reactions, branching ratios, radiation to space and many other parameters. One can easily conduct a large number of numerical simulations to develop an understanding of the important processes responsible for atmospheric structure and thus make it easier to transfer the important processes to other higher dimensional models.

A 1D model that was important for the development of the series of National Center for Atmospheric Research (NCAR) TGCMs was developed by Roble et al. (1987) for the thermosphere and ionosphere. It was further extended to include the mesosphere and upper stratosphere by Roble (1995). A thorough description of the model has been given in the 1995 paper. The model was designed to be fully consistent internally with only specification of temperature and composition at the lower boundary at 10 mb (30 km) and the upper boundary in thermal and diffusive equilibrium (500–700 km). It is a time dependent model generally run to steady state for global average forcing from solar EUV radiation, the aurora, and specified eddy diffusion. It was primarily used to develop the aeronomical scheme for the series of TGCMs and to test ideas and parameters. It has been used for numerous studies by colleagues and students to test various ideas. One example of a simulation for solar medium conditions is shown in Fig. 1.

This terrestrial 1D code has also been used to study global change in the upper atmosphere by Roble and Dickinson (1989) and more recently been used by Qian et al. (2006, 2008) to study decadal changes in satellite drag and ionospheric structure.

3.2 Venus and Mars

One-dimensional models have been constructed of the thermospheres and ionospheres of Mars and Venus since the first radio occultation measurements of the electron density profiles were reported from early flybys and orbiters. Lodders and Fegley (1998) have reviewed missions to these planets up to 1998.

There are two basic types of one-dimensional models: photochemical equilibrium (PCE) models, in which transport is ignored, and those that include (usually) vertical transport of species. While in the former type of model, the densities at each altitude can be computed independently, in the latter type of model numerical coupling of each altitude to those above and below it must be taken into account. Altitude profiles of neutral species in thermospheres cannot be modeled with the PCE approximation, although ion density profiles in the high density lower peak regions may be.

All of the early (and most of the subsequent) radio occultation electron density profiles measured by radio science experiments of both Mars and Venus have exhibited two peaks: an upper F1 peak, which is produced by absorption of the main portion of the EUV ($\sim$150–1000 Å), and a lower E peak which is produced by the absorption of soft X-rays (e.g., Kliore et al. 1967; Stewart 1971). Curiously, however, the ion density profiles derived from the Viking RPA measurements showed no lower peak (e.g., Hanson et al. 1977).

Most of the early models of the ionospheres of Mars and Venus that were designed to fit radio occultation electron density profiles, assumed PCE (e.g., McElroy 1967, 1968a, 1969; Stewart 1968, 1971). The Venus ionospheric model of Kumar and Hunten (1974), however, was a hybrid model, in which the heavy ions were assumed to be in PCE, while the lighter ions were subject to transport. Shimazaki and Shimizu (1970) constructed a number of models of the Martian ionosphere that included transport by diffusion and eddy diffusion, which were compared to the electron density profile measured by Mariner 4. Interestingly,

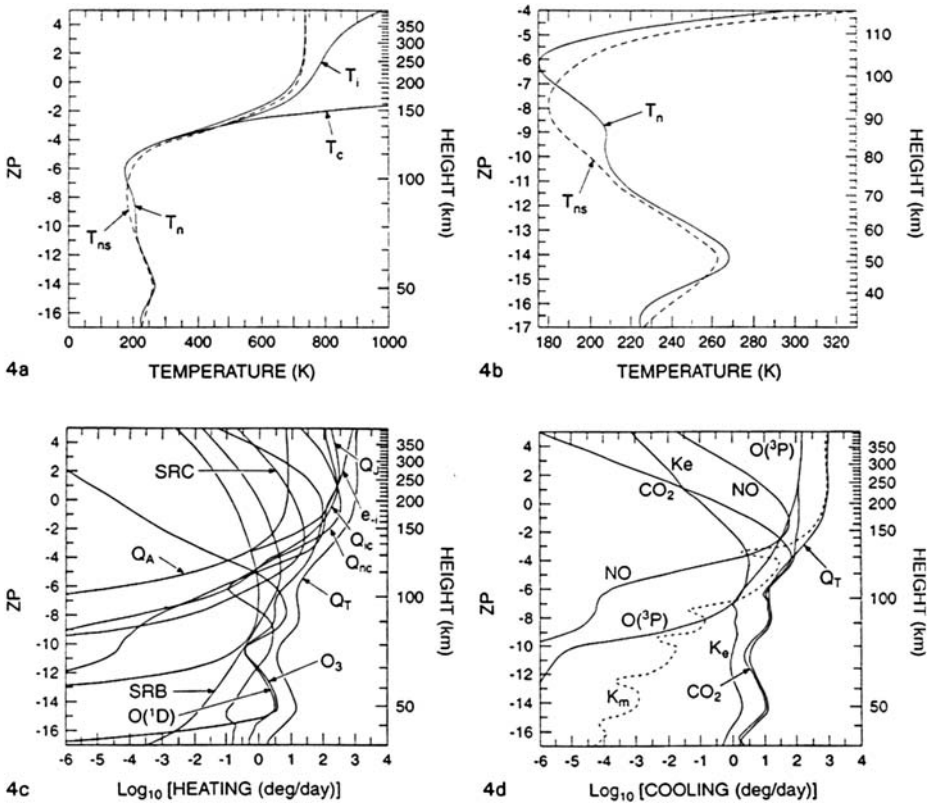

Fig. 1 NCAR 1D global mean model simulations for solar medium conditions. (**a**) Neutral, ion, and electron temperatures (∼30–400 km); (**b**) Neutral temperatures (40–120 km); (**c**) Heating terms of thermal equation (∼30–400 km); and (**d**) Cooling terms of the thermal equation (∼30–400 km). Individual curves for (**a**): Tn, Te, Ti: neutral, electron and ion temperatures; T_{ns}: neutral temperature from MSIS-90. Individual curves for (**c**): SRC: Schumann-Runge Continuum; SRB: Schumann-Runge Bands; Q_T: total heating; Q_J: Joule heating; Q_A: auroral heating; O_3: O_3 heating; $O(^1D)$: heating from $O(^1D)$ quenching; Q_{NC}: neutral chemistry heating; Q_{IC}: ion chemistry heating; Q_{EI}: ion–electron heating. Individual curves for (**d**): Q_T: total heating; K_e: cooling rates from eddy thermal conduction; CO_2: 15-micron cooling; NO: 5.3-micron cooling; K_m: cooling rate from downward molecular thermal conduction; $O(^3P)$: oxygen fine structure cooling. ZP (left vertical axis, log pressure scale used by the NCAR codes)

McElroy (1968b) noted the difficulty of constructing model ionospheres when the only information was in the form of radio occultation electron density profiles, without the benefit of *in situ* measurements of ion and neutral densities. The lack of *in situ* measurements has also plagued interpretation of the electron density profiles of the outer planets for many years.

The PCE approximation becomes inaccurate above the boundary where the lifetime of a species due to chemistry ($\tau_c = 1/L$), where $L = L/n$ is the specific loss rate, L is the total chemical loss rate and n is the number density of the species, becomes longer than that due to vertical transport. If the main transport process is by diffusion, the lifetime of a species due to transport is given approximately as $\tau_D \sim H^2/D$, where D is the diffusion coefficient of that species and $H = kT/mg$ is the scale height. In this expression, k is Boltzmann's constant, while T, g, and m are the altitude dependent temperature, acceleration of gravity, the mass

of the atmospheric species, respectively. For ions, the scale height is $H_i = k(T_i + T_e)/m_i g$, where T_i is the ion temperature, and T_e is the electron temperature.

If the major transport process (for neutrals) is mixing, the lifetime of a species against transport is given by $\tau_K \sim H_{avg}^2/K$, where K is the eddy diffusion coefficient, $H_{avg} = kT/m_{avg}g$, and m_{avg} is the average mass of the constituents. It is remarkable that the eddy diffusion coefficient is on the order of $1.0 \times 10^{13}/n^{0.5}$ cm^2 s^{-1}, where n is the total number density in the lower thermospheres for both Mars and Venus (cf., Krasnopolsky 1982; von Zahn et al. 1980).

The boundary where diffusion of a neutral species becomes more important than mixing is known as the homopause. In fact, however, that altitude is different for each species. In early models of the thermospheres of Venus and Mars, a single homopause altitude was assumed (e.g., McElroy 1967, 1969; Kumar and Hunten 1974; Chen and Nagy 1978). Below the homopause the thermosphere is considered to be completely mixed for chemical tracers/inert species; above the homopause, these species density profiles are assumed to be distributed according to their own scale heights. Species that are formed photochemically do not exhibit this behavior. Because of the availability of *in situ* measurements of the neutral densities, and the computing power that is available today, even in one-dimensional models, the homopause approximation is neither necessary nor used widely.

While PCE approximations are almost never used to compute the density profiles of minor neutral thermospheric species, such models of ion density profiles continue to be used for specific purposes, including studies focused on the electron density peak regions (e.g., Cravens et al. 1981; Fox and Dalgarno 1981; Kim et al. 1989; Martinis et al. 2003), or for airglow calculations of processes that originate near the electron density peaks (see, for example Fox 1992, and references therein).

The Viking I and II probes carried neutral mass spectrometers through the Martian atmosphere, and so the major neutral densities in the thermosphere at low solar activity were measured in situ for the first time (e.g., Nier and McElroy 1976). Early ionospheric models based on these measurements included, for example, those of McElroy et al. (1976), Fox and Dalgarno (1979), and Chen et al. (1978). While the latter model included vertical transport. The former two were photochemical equilibrium models. The *in situ* measurements of the Pioneer Venus orbiter and probes enabled more accurate models of the Venusian ionosphere (e.g., Chen and Nagy 1978; Nagy et al. 1980; Fox 1982).

In the terrestrial ionosphere, the absolute maximum in the electron density profile is an F_2 peak, which appears near 300 km. At this altitude, the chemical lifetime of the major ion (O^+) is approximately equal to that of transport. At high altitudes in the Venus ionosphere, O^+ becomes the most important species, yet models show that it forms a peak that is not (or is barely) visible in the electron density profile. On Mars, the O^+ density forms a peak at high altitudes, but thus far measurements indicate that densities of O^+ are everywhere smaller than those of O_2^+ (e.g., Hanson et al. 1977). Where the major loss is by transport, photochemical equilibrium models do not reproduce the profiles of ions, such as O^+ and other (mostly) atomic ions.

More sophisticated one-dimensional thermosphere/ionosphere models have included both chemistry and transport by molecular and eddy diffusion (for neutrals), and ambipolar diffusion (for ions), and do not assume a fixed homopause (e.g., Nagy et al. 1980; Fox 1982, 2004; Krasnopolsky 2002). The one-dimensional thermosphere-ionosphere models of Venus and Mars of Shinagawa and Cravens (1988, 1989) have also included magnetic fields.

Although one-dimensional models have limitations, mainly that horizontal transport by convection is ignored, they are simple enough that many species and reactions among those

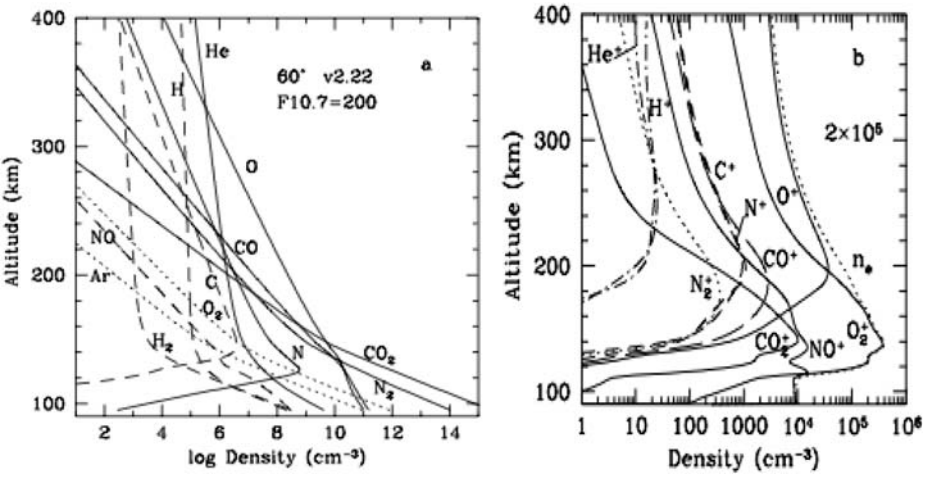

Fig. 2 Venus 1D simulations for solar maximum conditions: (**a**) Neutral densities; (**b**) ion densities and electron density. From Fox (unpublished)

species can be included in them. For example, the current Mars and Venus models of Fox and coworkers (e.g., Fox and Sung 2001; Fox 2004; Fox and Yeager 2006) contain 23 species and more than 200 reactions. These models include photoionization and excitation, photoelectron impact ionization and excitation, and electron-impact excitation of twelve neutral background species, and photodissociation, photodissociative excitation, and photodissociative ionization of all of the molecular neutral background species. Cross sections for all these processes are required input for the models.

An example of a one-dimensional Venus model for high solar activity is shown in Fig. 2. Figure 2a illustrates the background density profiles of 12 species; Fig. 2b shows the computed ion density profiles. In this model an upward velocity boundary condition of 2×10^5 cm s^{-1} was imposed on most ions, since the ionosphere of Venus is eroded by day-to-night ion transport. O^{++} ions are assumed to be in photochemical equilibrium. Using these models, density profiles of metastable species, such as $O^+(^2D)$, $O^+(^2P)$, $N(^2D)$, $N(^2P)$, $O(^1S)$, and $O(^1D)$ can be computed. These species can participate in reactions that are not available to ground state species, and are important to the energy balance in the thermosphere/ionosphere. Quenching of these species produces local heating, and radiation produces cooling. The radiation rates of shorter-lived excited species may be computed to produce profiles of airglow intensities.

Using one-dimensional models, the altitude-dependent heating efficiencies can be readily computed. The heating efficiency is defined as the ratio of the local heating rate to the solar energy absorbed at a given altitude. Computations show that for Mars and Venus (Fox 1988; Fox et al. 1995), the most important heat source near the ion peak is dissociative recombination of O_2^+,

$$O_2^+ + e \rightarrow O + O + \Delta E \tag{9}$$

where the product O atoms may be in various combinations of electronically excited states and the energy released Δ/E varies with the branching ratios (e.g., Kella et al. 1997). At low altitudes, photodissociation and quenching of metastable species are more important. Exothermic chemical reactions are of secondary importance, and electron impact is of minor

importance over the entire thermosphere. For Venus, the altitude dependent heating efficiencies range from about 16% at low altitudes for the "lower limit" model to 22% for the "best guess" model. At high altitudes the heating efficiencies increase slightly with altitude up to 185 km. On Mars, the "best guess model" yields heating efficiencies of about $21 \pm 2\%$ from 100 to 200 km, although at low altitudes the lower limit model shows heating efficiencies of about 16%.

4 Representative Multidimensional Models

4.1 Model Classes to be Addressed

Table 1 summarizes the classes of multi-dimensional models that we will consider in Sects. 4 and 5. Notice that multi-dimensional model development is following two important trends. First, existing upper atmosphere models are being extended to encompass the entire atmosphere domain (ground to exosphere) for Earth (NCAR WACCM) and Mars (Michigan-MWACM). The LMD-MGCM code for the Mars lower atmosphere has also be extended upward into the thermosphere. These efforts reflect the availability of both lower and upper atmosphere datasets for these planets. Coupling processes (thermal, chemical, dynamical) linking these atmospheric regions are important to address with these "whole atmosphere" modeling tools. Second, model frameworks are being developed and exercised using 8-moment and 13-moment solutions of the Boltzman equation. The motivations here are at least twofold: (a) to incorporate a non-hydrostatic treatment for improvement of the simulation of vertical velocities (Ridley et al. 2006; Deng et al. 2008), and (b) to capture the physical processes that bridge the collisional and non-collisional regions near the exobase (Boqueho and Blelly 2005).

Under hydrostatic equilibrium, a typical assumption used in most global planetary models, the pressure gradient in the vertical direction is exactly balanced by the gravity force (Deng et al. 2008). However, for large vertical velocities, acceleration terms in the vertical momentum equation cannot be ignored, and the basic balance is no longer hydrostatic. Two likely examples of these conditions are realized for the sudden intense enhancement of high latitude Joule heating for the Earth's thermosphere-ionosphere (Deng et al. 2008), and that of Jupiter as well. If the hydrostatic assumption is relaxed, the vertical momentum equation can be expanded to include additional acceleration terms: (1) forces due to ion-neutral and neutral-neutral friction (when each constituent is solved independently), (2) centrifugal and Coriolis forces, and (3) non-linear advection terms. The altitude variation of gravity is easily accommodated in this framework. Vertical propagation of a non-hydrostatic "disturbance" results in acoustic waves and non-hydrostatic gravity waves (Deng et al. 2008). Care must be taken to either damp or accommodate these waves in non-hydrostatic models. In short, global non-hydrostatic models are needed to address phenomenon associated with large vertical winds in planetary upper atmospheres. New planet specific global thermosphere–ionosphere models are being developed and validated for this purpose, based upon the Global Thermosphere–Ionosphere Model (GITM) for Earth (Ridley et al. 2006; Deng et al. 2008).

4.2 Representative GCM Model Descriptions/Results

4.2.1 Earth (NCAR TGCMs)

A series of TGCMs have been developed at NCAR over the past 30 years with each model incorporating new processes of the coupled thermosphere-ionosphere system. The histori-

cal development of the TGCM suite of models is discussed in Bougher et al. (2002). Self-consistent temperatures, neutral-ion densities, neutral dynamics, and self-consistent electrodynamics are contained in the TIE-GCM (Richmond et al. 1992). This code was then extended to include the mesosphere and upper stratosphere to become the TIME-GCM (Roble and Ridley 1994). These two codes are now the basic upper atmosphere models at NCAR. The TIE-GCM is used to explore thermosphere-ionosphere-electrodynamic interactions and the TIME-GCM has the same processes but extended to include aeronomic processes associated with the mesosphere and upper stratosphere and to examine physical and chemical interactions between upper atmospheric regions.

The TIME-GCM is a self-consistent model of the upper atmosphere extending between 30 km and 500 km altitude. It has been used for comparison and interpretation of satellite, rocket and ground-based data for many years by a wide variety of scientific colleagues, post doctoral fellows and graduate students. The TIME-GCM was initially designed for a 5° latitude and longitude grid in the horizontal and 2 grid points per scale height in the vertical with a 5 minute time step. This "coarse" horizontal and vertical resolution was later refined for specific model applications (see below). The TIME-GCM solves for the neutral gas temperature, winds and constituents of the thermosphere, mesosphere and upper stratosphere both major and minor species self-consistently. It also solves for the ionospheric plasma properties of electron and ion temperature, electron density and ion composition, and the electric field, plasma drift and resulting magnetic perturbations. The most recent description of the model is given by Roble (2000).

In the late 1990s, the TIME-GCM was extended to use lower boundary data at 10 mb (30 km) to force the variability propagating upward from the lower atmosphere and to study couplings between the lower and upper atmospheres (Roble 2000). This included specification of tides, gravity waves, planetary waves and other disturbances on a daily basis so that continuous simulations of the upper atmosphere could be made for realistic daily simulations that would be used to compare with observational time averaged campaign or satellite orbital tracking data.

In order to examine the feasibility of developing a model that extended from the ground-to-exosphere the TIME-GCM was flux coupled to the NCAR community climate model CCM3 (Khiel et al. 1998) at the boundary between the models near 10 mb. This allowed information between the upper and lower atmospheres to be exchanged simulating the entire atmosphere, troposphere, stratosphere, mesosphere and thermosphere/ionosphere. This coupled model simulated a strong stratospheric warming, mesospheric cooling, thermospheric warming at high latitudes that was generated spontaneously from planetary waves propagating upward from the troposphere (Liu and Roble 2002, 2005). These studies indicated that a continuous model from the ground to exosphere could be developed to examine coupling aspects between regions of the whole atmosphere. This was a precursor for the development of the WACCM that is discussed in Sect. 5.1.2.

The TIME-GCM resolution was limited by computer power in the 1990s and early 2000s. While this was sufficient for a number of upper atmosphere studies, it was inadequate to represent the shorter wave migrating and non-migrating tides and planetary wave propagation and dissipation. One temporary solution was to double the amplitudes of the Global Scale Wave Model (GSWM) forcing at the lower boundary to get agreement with observational data. Subsequent simulations showed that it was not necessary to double the amplitudes but rather to improve both the vertical (0.25 scale height) and horizontal (2.5° × 2.5°) resolution. These comparisons are shown in Fig. 3. With a double resolution, large tides developed without the need to double GSWM amplitudes. This exercise clearly illustrates the need to

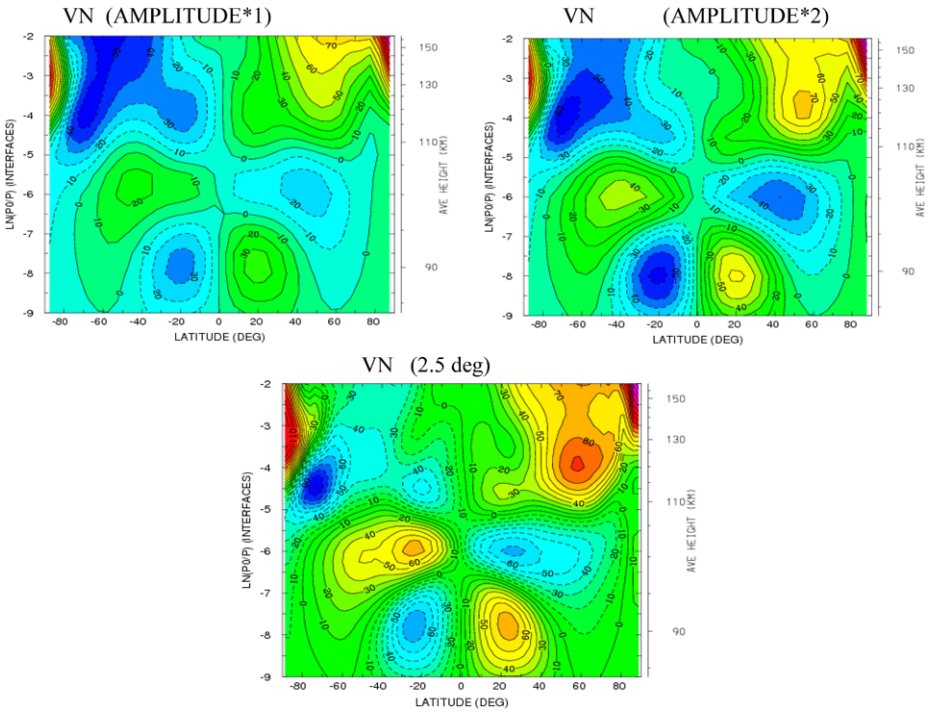

Fig. 3 NCAR TIME-GCM model simulations for solar moderate conditions. Meridional tidal winds (VN) in the ∼80–150 km region at local noon for: (**a**) standard GSWM forcing, (**b**) doubled GSWM forcing, and (**c**) standard GSWM forcing but with 2.5° horizontal resolution

match the model resolution (both vertical and horizontal) with the phenomena being examined. This new high-resolution model resolved a number of problems with simulation/data comparisons.

Work is continuing on evaluating the impact of the new resolution on a number of previous studies, such as the migrating and non-migrating tides, auroral dynamics, thermospheric densities and satellite drag and ionospheric F-region dynamics as well as a number of airglow studies. A web site that describes the model and some important simulations is: http://www.hao.ucar.edu/modelling/tgcm/tgcm.html.

Validation of other planetary GCM codes (see Sects. 4.2.2–4.2.9) may also require sensitivity tests to confirm the model resolution necessary to obtain converged solutions; i.e. finer vertical (e.g. ∼0.25 scale height) and horizontal (e.g. 2.5° × 2.5°) resolution may also be required to obtain converged solutions for important desired applications.

4.2.2 Earth (CTIM, CTIP, CMAT codes)

Another major atmosphere general circulation model for Earth is the CTIP model developed jointly by groups in the UK and US. The code originates from two initially separate models for the thermosphere (Fuller-Rowell and Rees 1980, 1983) and high latitude ionosphere (Quegan et al. 1982) which were later coupled (Fuller-Rowell et al. 1987, 1996) for two-way coupling between the neutral and ionized regimes of the upper atmosphere, a version of the model often referred to as CTIM. A self-consistent plasmasphere model for the regions

equatorward of around 30° geomagnetic latitude was added by Millward et al. (1996a) to form CTIP. More recently, the original bottom boundary (80 km, 0.01 mb) of the CTIM model was lowered by Harris (2001) into the stratosphere (30 km, 10 mb) in order to include the stratospheric and mesospheric chemistry and full vertical dynamical and chemical coupling. This extended version of the model is referred to as the CMAT model.

What distinguishes these from other thermosphere/ionosphere models is primarily the fact that ionospheric calculations are carried out along magnetic field lines rather than being treated on the same spherical grid as the neutral gases. This has proven to be a most useful approach since one key issue is how to treat upper boundary conditions for ions and electrons, in particular the plasma fluxes along field lines in the topside ionosphere where field-aligned transport forms a dominant process affecting the distribution of O^+ and H^+ ions and electrons. The plasma flux boundary condition becomes important for calculations of ionospheric densities when the boundary is located within a few scale heights above the density peak. The particular choice of flux tube coordinates for plasma in CTIP/CTIM eliminates this difficulty. At high latitudes field lines are open and extend to around 10000 km altitude in the model, while at low latitudes flux tubes in CTIP are closed. With plasma densities near 10000 km being negligible compared with ionospheric densities, a zero flux boundary condition can safely be assumed, while in the regime of closed flux tubes both ends of a field line are within the photochemical domain of the ionosphere (in opposite hemispheres), allowing the simple boundary condition of photochemical equilibrium.

The CTIP, CTIM and CMAT models have been used extensively over the past decades to understand the global morphology of the thermosphere and ionosphere both through purely theoretical studies and in comparisons with observations. Studies have investigated (amongst others) the morphology of responses to geomagnetic storms (Field et al. 1998; Fuller-Rowell et al. 2002), thermospheric composition and dynamics (Fuller-Rowell 1998; Rishbeth and Mueller-Wodarg 1999), semiannual variations in the ionosphere (Millward et al. 1996b; Rishbeth et al. 2000a), effects of tidal forcing (Millward et al. 2001; Mueller-Wodarg et al. 2003) and NO chemistry (Dobbin et al. 2006).

4.2.3 Michigan GITM Codes

Earth GITM. The GITM code (Ridley et al. 2006) was designed from the bottom up with flexibility in mind for every aspect of modeling upper atmospheres of planetary systems. The grid system within GITM is fully parallel and is quite versatile. Users can run 1D cases at a specified latitude and longitude (which is set at run-time in the input file) or 3D cases with almost any latitudinal and longitudinal resolution that the user wants (once again, set at run-time). GITM can run on a single processor machine or multi-processor machines. It has been run on 256 processors resolving the upper atmosphere with a 1.25° latitudinal by 2.5° longitudinal resolution. For testing, GITM has been run with 10° by 20° resolution. This flexibility in the resolution allows rapid development of the model and facilitates testing of new physics within the code.

The main feature that differentiates GITM from all other coupled ionosphere thermosphere models is the easing of the hydrostatic assumption within the vertical momentum equation—the pressure does not have to balance with gravity (although it almost always does). In regions in which there are non-hydrostatic forces (e.g., the auroral zone), large vertical winds can develop (Deng et al. 2008). In addition, the GITM vertical momentum equation allows gravity to be dependent on altitude, instead of constant, which is crucial for small bodies with extended atmospheres, such as Titan. GITM utilizes an altitude grid, which is also different than other upper atmosphere models. The resolution in the vertical direction is stretched such that it is approximately $1/3$ of a scale height at code initiation.

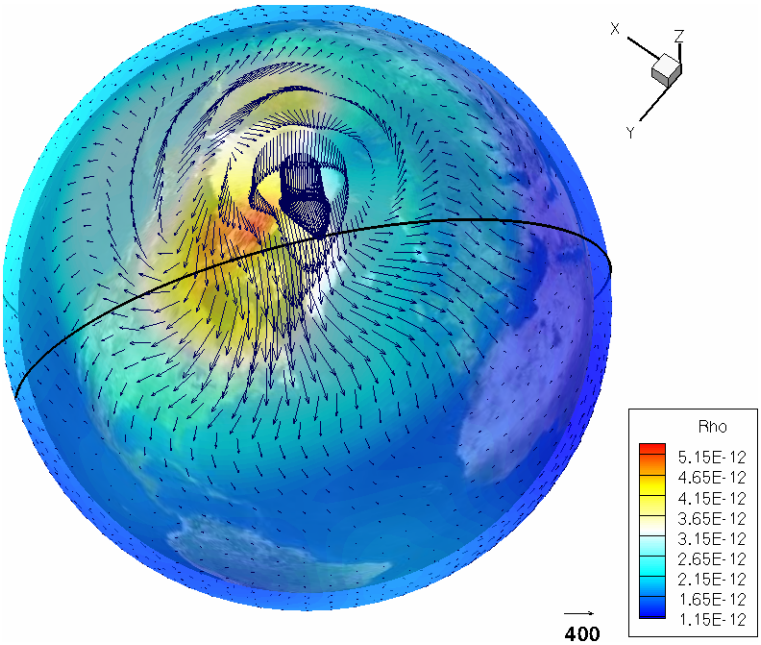

Fig. 4 Earth GITM simulation at 400 km. Horizontal wind vectors are superimposed upon mass density color contours (1.15 to 5.15 $\times$ 10^{-12} g/m^3)

An additional feature of GITM is the ability to turn on and off physics through the input file. Different source terms (such as Coriolis, Joule heating, solar EUV heating, and thermal conduction), can be turned off through the input file. This allows users to conduct numerical experiments in which they self-consistently determine the effects of different source terms on the coupled nonlinear system.

In order to allow GITM to be utilized for more than a single body, very little was hard-coded into the core of GITM. Each atmospheric and ionospheric constituent is specified in a planet specific module, such that the advective core need only loop over the number of species to determine the hydrodynamic behavior of the atmosphere. Other common source terms, such as solar EUV inputs, and inter-species frictional drag in the vertical direction, are handled in a similar manner, allowing the code to be adapted to another planet very easily. More specific source terms, such as radiative cooling, need to be coded for the particular problem and are easily linked to GITM through hooks.

At Earth, GITM has an extremely flexible high-latitude energy input module. This allows users to try different electric fields and particle inputs to drive GITM. At other planets, this can be easily adapted to different types of forcing. Models of electron precipitation and electric potential can be added with little difficulty. These will then be utilized to calculate electric fields and ion and electron velocities. Joule heating and ion-neutral momentum coupling are then self-consistently calculated.

Figure 4 shows results from the Earth-based GITM at 400 km altitude. The vectors show the thermospheric neutral winds, while the coloring is the thermospheric mass density. The neutral winds roughly follow a two-cell convection pattern at high latitudes, due to the strong forcing by the ion convection and aurora. On the dusk-side (left), the neutrals are able to form a completely closed cell, while on the dawn-side (right), the cell is less well defined.

This is because on the dusk-side, the Coriolis force is in the same direction as the circulation pattern, so the closed cell is accentuated, while on the dawn-side, the flow is inhibited, since the Coriolis force opposes it. At very high latitudes and at the tail end of the convection cells on the night side (i.e., just over Canada), there is a large enhancement in the thermospheric mass density. This is caused by Joule heating in the auroral zone, where there are extremely large electric fields and strong conductivities. During this strong driving period, the density peaks at the poles, while during quieter times, the mass density peaks at lower latitudes.

Titan GITM. A new application of the GITM framework was recently developed (Bell et al. 2006; Bell 2008) in an effort to interpret and place in a global context new Cassini INMS neutral and ion density and inferred temperature datasets of the Titan upper atmosphere (e.g., Waite et al. 2005). The GITM framework was chosen to capture the unique physics of the Titan upper atmosphere that requires: (a) variable gravity, (b) calculated fluxes of major species out the top of the atmosphere, and (c) variable Saturn magnetospheric forcing. Density gradients (yielding fluxes) were specified at the upper boundary in order to simulate measured Cassini INMS CH_4 density profiles; the self-consistent feedback of these fluxes upon temperatures was also included. The Titan GITM code was designed to span ∼500 to 1500 km in the Titan upper atmosphere, covering the region below the homopause (∼800 km) to just above the exobase (∼1300 km). Solar EUV forcing (heating, photo-dissociation, photo-ionization) is dominated by N_2 and CH_4 solar absorption between 1.6–170.0 nm. Hydrogen cyanide (HCN) rotational band infrared radiative cooling is incorporated and represents the dominant IR cooling agent in the thermosphere. A self-consistent treatment of chemical production and loss processes for 4-major, 7-minor, several isotopes, and thermally active (e.g. HCN) constituents is incorporated, based upon the scheme outlined by DeLa Haye (2005). Major photochemical ions are limited to key species: N_2^+, N^+, CH_3^+, H_2CN^+, and $C_2H_5^+$. Finally, a differentially, super-rotating lower boundary is specified at ∼500 km, in accord with ground-based observations (Hubbard et al. 1993). Horizontal and vertical distributions of simulated temperatures and densities have been successfully compared to specific Cassini orbit measurements, especially profiles of key isotopes (e.g., Bell 2008).

Mars GITM. The need for a ground-to-exobase GCM at Mars has motivated another new application of the GITM framework. Existing Mars lower and upper atmosphere datasets need to be interpreted and connected using such a "whole atmosphere" model framework (e.g., Bougher et al. 2006b). This is the first extension of the GITM framework over a wide range of altitudes encompassing both upper and lower atmosphere processes.

A prototype MWACM code using the GITM framework has been developed, enabling initial 1D and 3D simulations to be conducted over 0–300 km for specific solar cycle, seasonal and dust conditions at Mars. Specifically, the terrestrial GITM code (Ridley et al. 2006) was adapted to include Mars fundamental parameters, constants, and key radiative processes in order to capture the basic observed features of the thermal and dynamical structure of the Mars atmosphere from the ground to 300 km. For the Mars lower atmosphere (0–80 km), an efficient (fast) radiation code was adapted from the NASA Ames MGCM code to the framework of the MWACM. This now provides MWACM solar heating (long and short wavelength), aerosol heating, and CO_2 15-micron cooling in the LTE region of the Mars atmosphere below ∼80 km. For the Mars upper atmosphere (∼80 to 300 km), a fast formulation for NLTE CO_2 15-micron cooling was implemented into the MWACM code, along with a correction for non-LTE (NLTE) near-IR heating rates (∼80–120 km). In addition, a thermospheric EUV-UV heating routine (based upon a CO_2 dominated atmosphere) was adapted to the MWACM framework. Finally, detailed neutral-ion chemistry was recently incorporated above 80 km, based upon Mars TGCM reactions and rates (see Sect. 4.2.5).

For the entire atmosphere, the MWACM dynamical core solver was modified to work with the new terrain following coordinate system. The Martian terrain is now being incorporated into the MWACM code making use of Mars Global Surveyor MOLA topographic data files. NASA Ames MGCM CO_2 condensation, and boundary layer routines will be added below 80 km. At the surface, global empirical maps of albedo and thermal inertia will be supplied to the radiation calculations. Initial simulations indicate this extended model is stable and captures the basic observed temperatures and expected wind structures throughout the Mars atmosphere.

4.2.4 Venus (NCAR VTGCM)

The large-scale circulation of the Venus upper atmosphere from ∼90 to ∼200 km (upper mesosphere and thermosphere) is a combination of two distinct flow patterns: (1) a relatively stable subsolar-to-antisolar (SS-AS) circulation cell driven by solar (EUV-UV-IR) heating, and (2) a highly variable retrograde superrotating zonal (RSZ) flow (see reviews by Bougher et al. 1997, 2006a, 2006b; Schubert et al. 2007). GCMs have proven useful for synthesizing the available Pioneer Venus, Magellan, Venus Express, and ground-based density, temperature, and/or airglow datasets and thereby extracting these upper atmosphere wind components (see reviews by Bougher et al. 1997, 2006a; Schubert et al. 2007).

The Venus TGCM (VTGCM) is a 3D finite difference hydrodynamic model of the Venus upper atmosphere that is based on the NCAR terrestrial TGCM. The VTGCM has been documented in detail as revisions and improvements have been made over nearly 2-decades (see Bougher et al. 1988, 1990, 1997, 1999a, 2002; Bougher and Borucki 1994; Zhang et al. 1996).

The modern VTGCM code (e.g., Brecht et al. 2007; Rafkin et al. 2007; Bougher et al. 2008) calculates global distributions of major species (CO_2, CO, O, and N_2), minor species (e.g. O_2, NO, $N(^4S)$, $N(^2D)$), and dayside photochemical ions (CO_2^+, O_2^+, O^+, and NO^+). These constituent fields are all consistent with the simulated 3-D temperature structure and the corresponding 3-component neutral winds. The VTGCM model covers a 5° by 5° latitude-longitude grid, with 46 evenly spaced log-pressure levels in the vertical, extending from approximately ∼80 to 200 km at local noon. Dayside O and CO sources arise primarily from CO_2 net dissociation and ion-neutral chemistry; the latter utilizes the ion-neutral chemical reactions and rates of Fox and Sung (2001). Simplified catalytic ClOx and HOx reactions can also employed to specifically improve the chemical sources and sinks for O and CO below 120 km (e.g., Bougher and Borucki 1994).

Formulations for CO_2 15-micron cooling, wave drag, and eddy diffusion are incorporated into the VTGCM (see Bougher et al. 1999a; Brecht et al. 2007). In particular, CO_2 15-micron emission is known to be enhanced by collisions with O atoms, providing increased cooling in NLTE regions of the upper atmosphere (see Bougher et al. 1994; Kasprzak et al. 1997). VTGCM CO_2 15-micron cooling is parameterized as described by Bougher et al. (1986), making use Roldan et al. (2000) exact cooling profiles at reference temperatures and atomic oxygen abundances. The collisional O–CO_2 relaxation rate adopted for simulated 15-micron cooling is $\sim 3 \times 10^{-12}$ cm^3/s. In addition, near-IR heating rates are incorporated using modern offline look-up tables from Roldan et al. (2000). These parameterizations provide strong CO_2 15-micron cooling that is consistent with the use of EUV-UV heating efficiencies of ∼20–22%, which are in agreement with detailed offline heating efficiency calculations of Fox (1988).

The VTGCM is typically run to examine Venus thermospheric structure and winds for solar maximum, moderate, and minimum EUV-UV flux conditions, corresponding to terrestrial F10.7-cm indices of 200, 110-130, and 68-80, respectively. In addition, the VTGCM

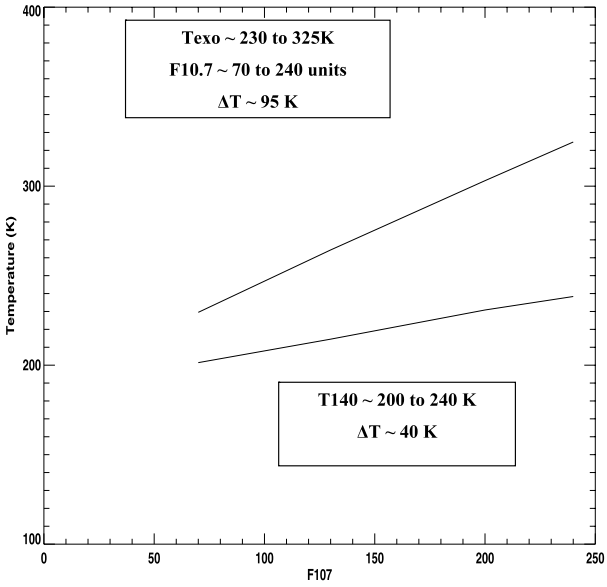

Fig. 5 VTGCM predicted exospheric temperature variations for dayside, equatorial conditions. $\Delta Texo \sim 95$ K for ΔF 10.7∼170 units. $Tmax = 325$ K; $Tmin = 230$ K. Temperatures at 140 km are also plotted: ∼200 to 240 K

is designed to calculate O_2 visible (400–800 nm), O_2 IR (1.27 microns) and NO ultraviolet (198.0 nm) nightglow distributions for comparison with various Venera, Pioneer Venus, Venus Express, and/or ground-based measurements (e.g. Bougher et al. 1997, 2006a, 2008; Brecht et al. 2007). These night airglow layers, and the controlling global circulation patterns being traced, span ∼90 to 150 km. Figure 5 illustrates the VTGCM predicted dayside, equatorial exospheric temperature variation, in substantial agreement with available Pioneer Venus and Magellan observations (e.g., Keating et al. 1980; Keating and Hsu 1993; Kasprzak et al. 1997). Figure 6 illustrates the VTGCM exobase circulation pattern and the underlying asymmetric thermospheric temperature structure for solar moderate conditions. Night airglow distributions respond to this mean circulation pattern, with maxima that occur on average near (or just beyond) midnight and close to the equator (e.g., Bougher et al. 2006a, 2008).

However, existing GCMs are presently unable to reproduce the significant variations in observed diurnal density, temperature, and airglow fields utilizing a unique set of wind fields, eddy diffusion coefficients, and wave drag parameters (Bougher et al. 1997, 2006a). This problem may reflect missing physical processes or inputs, e.g., exospheric transport above 180–200 km, upward propagating planetary waves, and limited gravity wave constraints for formulating wave breaking (Bougher et al. 2006a).

4.2.5 Mars (NCAR MTGCM)

The Mars TGCM (MTGCM) is a finite difference primitive equation model that self-consistently solves for time-dependent neutral temperatures, neutral-ion densities, and three component neutral winds over the Mars globe (e.g., Bougher et al. 1999a, 1999b, 2000, 2002, 2004, 2006b; Bell et al. 2007). The MTGCM code is adapted from the NCAR TGCM framework (see Sect. 4.2.1).

The modern MTGCM code contains prognostic equations for the major neutral species (CO_2, CO, N_2, and O), selected minor neutral species (Ar, NO, $N(^4S)$, O_2), and several photochemically produced ions (e.g. O_2^+, CO_2^+, O^+, and NO^+ below 180 km). All fields are

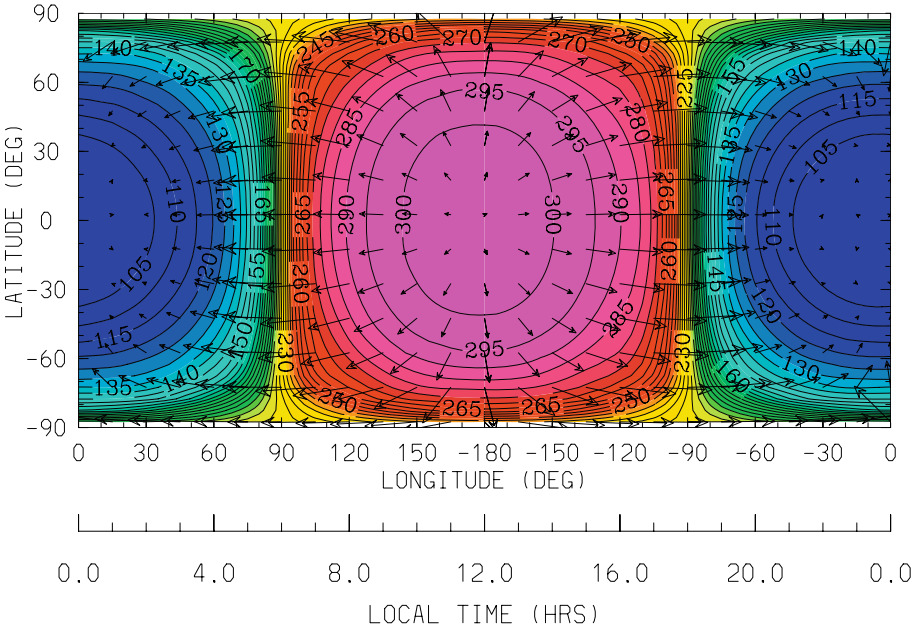

Fig. 6 VTGCM simulated exospheric temperatures and superimposed horizontal neutral winds for Equinox, $F10.7 = 200$ conditions (similar to early Pioneer Venus observations). Dayside equatorial temperatures reach ∼305 K. Nightside minimum temperatures drop to ∼100 K. Maximum horizontal winds reach ∼220 m/sec (∼70–90% of the sound speed in the upper thermosphere) across the evening terminator. The average altitude for this slice is ∼180 km

calculated on 33 pressure levels above 1.32 μbar, corresponding to altitudes from roughly 70 to 300 km (at solar maximum conditions), with a 5° resolution in latitude and longitude. The vertical coordinate is log pressure, with a vertical spacing of 0.5 scale heights. Key adjustable parameters which can be varied for MTGCM cases include the $F10.7$-cm index (solar EUV/UV flux variation), the heliocentric distance and solar declination corresponding to Mars seasons. A fast NLTE 15-micron cooling scheme is implemented in the MTGCM, along with corresponding near-IR heating rates (Bougher et al. 2006b). These inputs are based upon detailed 1D NLTE model calculations for the Mars atmosphere (e.g., López-Valverde et al. 1998).

A simple dayside photochemical ionosphere is formulated for the MTGCM, including the major ions. Key ion-neutral reactions and rates are taken from Fox and Sung (2001); empirical electron and ion temperatures are adapted from the Viking mission for various solar conditions. The ionization rates required for the production rates are calculated self-consistently, making use of specified solar EUV fluxes. Nightside ions are not yet simulated, but will require either day-to-night ion drifts from modern magnetohydrodynamic models (e.g., Ma et al. 2004), or energetic electron precipitation sources of nightside ionization (e.g., Fillingim et al. 2007).

The MTGCM is driven from below by the NASA Ames Mars MGCM code (Haberle et al. 1999) at the 1.32-μbar level (near 60–80 km). This coupling allows both the migrating and non-migrating tides to cross the MTGCM lower boundary and the effects of the expansion and contraction of the Mars lower atmosphere to extend to the thermosphere. The entire atmospheric response to simulated dust storms can also be calculated using these coupled

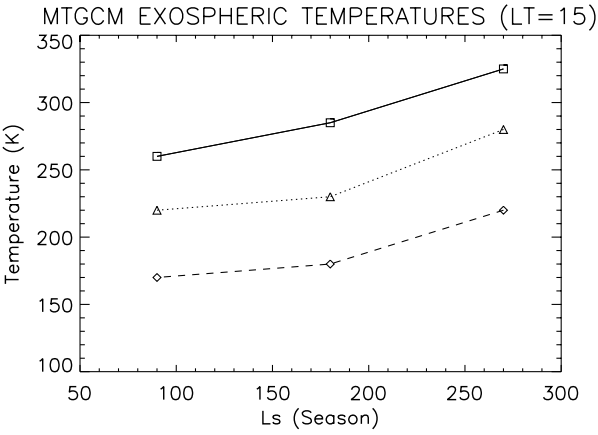

Fig. 7 MTGCM exospheric temperatures as a function of *Ls* (season) and solar cycle ($F10.7$-cm index). Dayside ($LT = 1500$) equatorial conditions are displayed. Curves indicated: $F10.7 = 175$–200 (*top*), 110–130 (*middle*), and 70–80 (*bottom*)

models. Key prognostic variables are passed upward from the MGCM to the MTGCM at the 1.32-μbar level at every MTGCM grid point: temperatures, zonal and meridional winds, and geopotential heights. These two climate models are each run with a 2-minute time step, with the MGCM exchanging fields with the MTGCM at this frequency.

This coupled configuration has been validated using an assortment of spacecraft observations, including Mars Global Surveyor, 2001 Mars Odyssey, and Mars Reconnaissance Orbiter thermosphere and/or ionosphere data sets (Bougher et al. 1999b, 2000, 2004, 2006b). Figure 7 shows dayside, equatorial exospheric temperature variations predicted by the MTGCM over the solar cycle and Mars seasons. These variations are in reasonably good agreement with available aerobraking and orbital drag measurements (e.g., Keating et al. 1998, 2003; Forbes et al. 2008; Mazarico et al. 2007). Exobase neutral horizontal winds and temperatures for solar maximum, southern summer solstice conditions are also illustrated in Fig. 8. In general, the global wind patterns simulated by the MTGCM reveal very strong summer-to-winter inter-hemispheric Hadley circulations that are consistent with observed NO nightglow (Bertaux et al. 2005) and winter polar warming (Bougher et al. 2006b) features. Finally, no downward coupling is presently activated between the MGCM and the MTGCM. However, the impacts of lower atmosphere dynamics upon the upper atmosphere are dominant (see Sect. 5.1.3).

4.2.6 Jupiter (JIM)

The JIM code is a general circulation model calculating the global thermosphere and ionosphere on Jupiter above the 2 μbar level (set to 357 km above the 1 bar level). This model, the first of its kind for Jupiter, was developed in the UK by Achilleos et al. (1998) and based largely on the thermosphere model of CTIM (see Sect. 4.2.2). Solar heating and photoionization are calculated self-consistently by solving the Beer–Lambert law. The thermospheric dynamics are calculated assuming all non-linear terms in the momentum equation, including ion drag, and ion dynamic calculations include diffusion and neutral drag. Calculations of the distribution of major neutral species H, H_2 and He include transport by winds and diffusion as well as simple ion-neutral photochemistry above the homopause. Unlike CTIM, ions in JIM are calculated on the same spherical pressure grid as the neutrals, which assumes a 10° horizontal resolution. The principal ions considered are H^+, H_2^+ and H_3^+, with more complex organic molecules which occur mainly below the homopause being

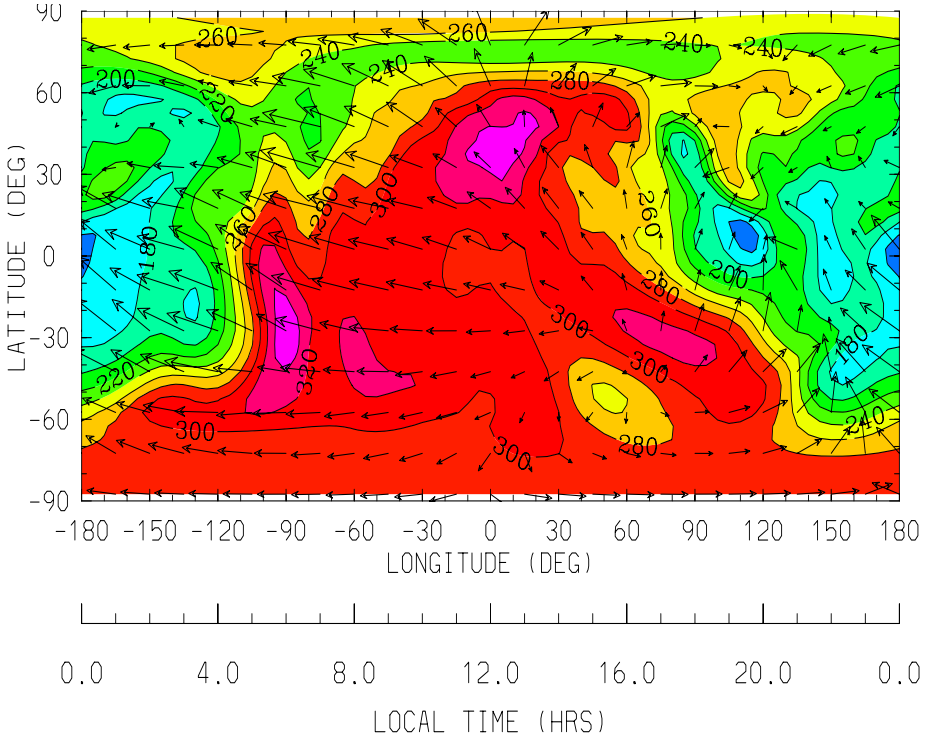

Fig. 8 MTGCM simulated exospheric temperatures and superimposed horizontal neutral winds for $Ls = 270$, $F10.7 = 175$ conditions (similar to late Mars Odyssey aerobraking observations). Dayside subsolar latitude (~25 S) temperatures reach ~320 K, nightside minimum temperatures drop to ~145 K. Maximum horizontal winds reach ~550 m sec^{-1} (slightly in excess of the sound speed). The average altitude for this slice is ~215 km

treated through a generic single molecule in the ion recombination reactions. A magnetic field is included for the calculations of ion dynamics and transport. In the auroral zones JIM allows for the inclusion of particle precipitation from the magnetosphere to calculate ionization and energy deposition. At high latitudes an electric field is included to simulate the auroral electrojet (Achilleos et al. 2001). Studies with JIM have helped investigate the morphology of thermosphere ionosphere coupling on Jupiter, in particular the dynamics at high latitudes (Millward et al. 2005), electrodynamic coupling between the thermosphere and the auroral ionosphere (Achilleos et al. 2001) and ionospheric conductivities (Millward et al. 2002a, 2002b).

4.2.7 Jupiter (NCAR JTGCM)

The proper characterization of Jupiter's upper atmosphere, embedded ionosphere, and auroral features requires the examination of underlying processes, including the feedbacks of energetics, neutral-ion dynamics, composition, and magnetospheric coupling. Coupled thermosphere and ionosphere GCM models (with magnetospheric inputs) can be used to address these feedbacks.

A Jupiter TGCM (JTGCM) code has now been developed and exercised to address global temperatures, three-component neutral winds, and neutral-ion species distributions

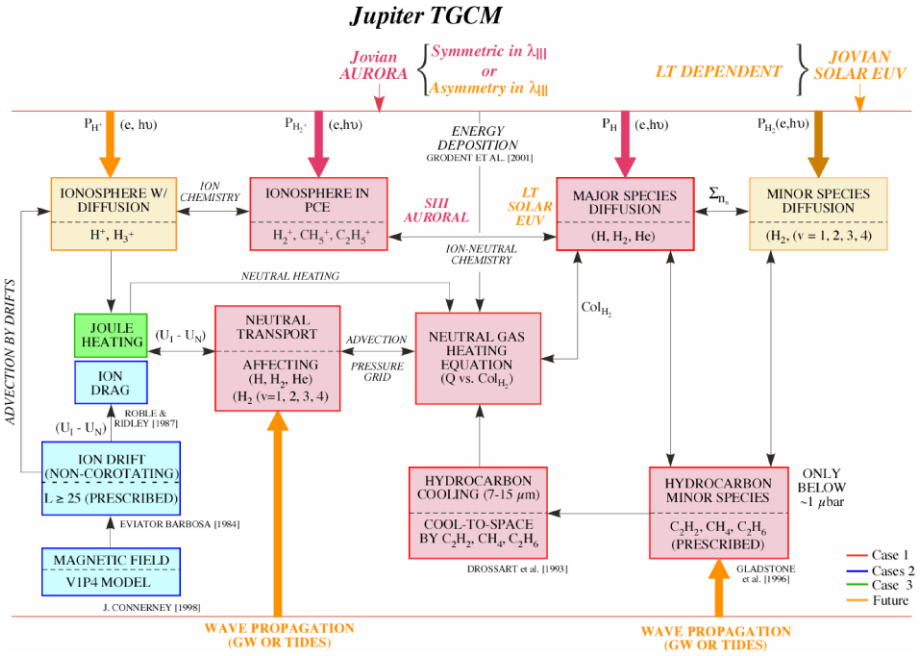

Fig. 9 JTGCM. This schematic summarizes the various thermosphere, ionosphere, magnetosphere processes and their couplings that are presently incorporated into the JTGCM code. Case 1 (auroral forcing alone), Case 2 (auroral forcing plus moderate ion drag/Joule heating), and Case 3 (auroral forcing plus strong ion drag/Joule heating) processes are identified corresponding to JTGCM simulations presented in Bougher et al. (2005). Future planned upgrades and processes are also indicated (*orange shading*)

(Bougher et al. 2005; Majeed et al. 2005, 2008). This code is based upon the NCAR TIE-GCM framework. Neutral temperatures, 3-component neutral winds, major neutral species (H, H_2, He), and major ion species (H^+, H_2^+, H_3^+) are simulated. The domain of this JTGCM framework extends from 20-mbar (capturing hydrocarbon cooling) to $\sim 1.0 \times 10^{-4}$ nbar (including auroral and Joule heating processes). A $5 \times 5°$ horizontal grid is utilized, along with a 0.5 scale height vertical resolution. Auroral and Joule heating processes are incorporated, both of which contribute to maintaining the neutral temperatures and driving the global winds. Joule heating is produced by the action of a prescribed plasma drift pattern that is consistent with the convection electric field derived from the Voyager constrained magnetospheric model of Eviatar and Barbosa (1984). Simulated auroral electrojet ion wind magnitudes approach ~1.5–3.0 km sec^{-1}. The benchmark JTGCM was fully spun-up and integrated for >50 Jupiter rotations, thereby achieving steady state solutions above the ~1.0-μbar level.

Initial results from three JTGCM cases incorporating moderate realistic auroral heating, ion drag, and moderate to strong Joule heating processes were presented by Bougher et al. (2005). Figure 9 summarizes the various thermosphere-ionosphere-magnetosphere processes and their couplings that are presently incorporated into the JTGCM code. The neutral horizontal winds at ionospheric heights vary from ~0.5 km s^{-1} to 1.2 km s^{-1} (approaching the sound speed), atomic hydrogen is transported equatorward, and auroral exospheric temperatures range from ~1200–1300 K to above 3000 K, depending on the magnitude of Joule heating. Figure 10 shows JTGCM simulated equatorial temperature profiles, and comparisons with multispectral and Galileo ASI observations (Majeed et al. 2005). The

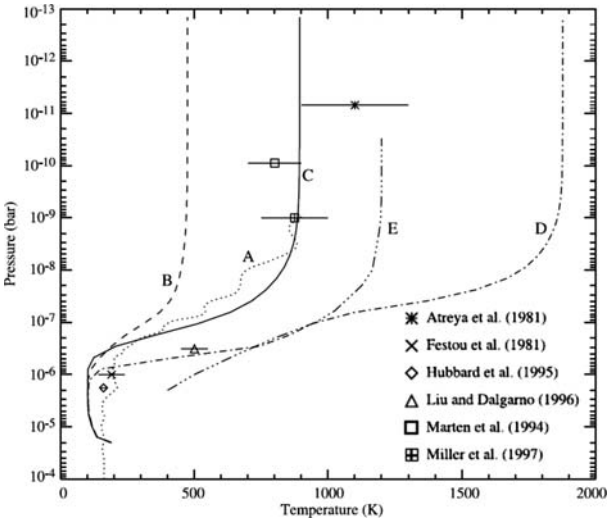

Fig. 10 JTGCM equatorial temperature profiles are shown in comparison with corresponding temperature profiles from JIM (*curve E*) and in-situ measurements from the Galileo ASI probe (*curve A*). *Curve B* assumes JTGCM auroral heating alone (no Joule heating). *Curve C* is from the "best" JTGCM simulation that incorporates auroral plus 15% joule heating conditions. *Curve D* is from the JTGCM simulation that assumes auroral plus 30% joule heating conditions. Remotely sensed (multi-spectral) temperature observations are also displayed (see key). From Majeed et al. (2005)

best fit to the Galileo data implies that the major energy source for maintaining the equatorial temperatures is due to dynamical heating induced by the low-latitude convergence of the high-latitude-driven thermospheric circulation. Simulated Joule heating can be quite large, requiring a scaling factor (∼15%) to enable both observed equatorial and auroral oval temperatures to be simulated (Majeed et al. 2005, 2008). Overall, the Jupiter thermosphere/ionosphere system is highly variable and is shown to be strongly dependent on magnetospheric coupling that regulates Joule heating.

Diagnostic heat balance studies utilizing the JTGCM have been employed to quantify in detail the thermal balance processes required to maintain thermospheric temperatures consistent with multi-spectral observations of Jupiter's equatorial (Majeed et al. 2005), auroral oval and polar cap regions (Majeed et al. 2008). It is found that upwelling/divergent winds in the auroral oval regions provide local cooling (reducing temperatures from values otherwise expected using 1D models), while downwelling/convergent winds in the equatorial region provide local heating largely responsible for maintaining the warm temperatures measured. In general, the significant Jovian auroral plus Joule heating processes appear sufficient to drive a strong equatorward (meridional) flow that is adequate to overcome Coriolis forces and to dynamically produce warm equatorial temperatures. This ability of Jovian equatorward winds to overcome Coriolis forces is apparently different than for Saturn (Mueller-Wodarg et al. 2006), where the combined auroral plus Joule heating magnitudes at polar latitudes are reduced from those at Jupiter (Strobel 2002). Correspondingly, Jovian auroral and Joule heating at polar latitudes combine to drive local heating and corresponding dynamical cooling, together controlling the thermal structure of the ovals and the polar cap regions. These results are beginning to address the "heat budget problem" of the Jovian upper atmosphere that has been debated for decades (c.f. Yelle and Miller 2004).

4.2.8 Saturn (STIM)

The first general circulation model of Saturn's thermosphere and ionosphere was presented by Mueller-Wodarg et al. (2006) and is referred to as the STIM code. The model forms part of a collaborative project between Boston University, Imperial College London and

University College London. It calculates the response of Saturn's upper atmosphere to solar heating and ionization, including global dynamics, composition and the thermal structure. The coupled non-linear equation of momentum, energy and continuity are solved on a global spherical pressure level grid above the 100 nbar level (800 km above the 1 bar level). Horizontal and vertical resolutions are flexible, allowing them to be optimized for specific problems under investigation. A simplified scheme of ion and neutral photochemistry is included and recent additions include ion diffusion and full ion-neutral dynamical coupling. The model has been used to investigate the thermal balance on Saturn in order to investigate the origin of abnormally large thermospheric temperatures on Saturn and other gas giants. It was found that the fast rotation of Saturn and strong Coriolis forces prevented energy deposited at auroral latitudes in the form of Joule heating from propagating equatorward and explain the observed low latitude thermosphere temperatures (Mueller-Wodarg et al. 2006; Smith et al. 2005), as shown in Fig. 11. The importance of global dynamics for understand-

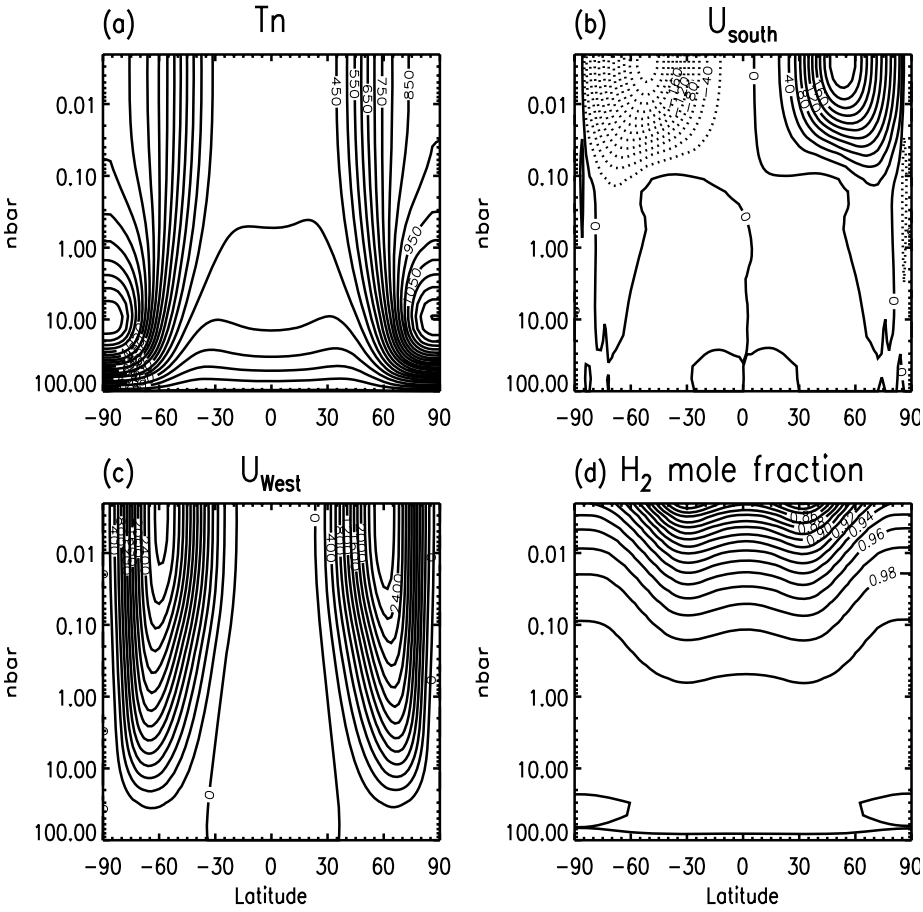

Fig. 11 Diurnally averaged temperatures, horizontal winds and H_2 mixing ratios versus latitude and height for equinox and solar maximum conditions, as calculated by the STIM GCM. The simulation considers Joule heating in the auroral regions. U_{South} and U_{West} are meridional and zonal winds, respectively, defined as positive southward and westward

ing the thermal balance on gas giants such as Saturn makes the use of general circulation models particularly relevant there. Other studies with the ionospheric module of STIM investigated the global structure of Saturn's highly variable ionosphere, considering shadowing by Saturn's rings (Moore et al. 2004) and effects of water precipitating into Saturn's ionosphere from the rings (Moore et al. 2006). These calculations found the presence of water to be important to reproduce the dawn dusk asymmetries in electron densities observed by the Cassini Radio Science experiment (Nagy et al. 2006). A recent study by Moore and Mendillo (2007) proposed variable water influx rates to be responsible for the high variability of Saturn's ionospheric densities.

4.2.9 Titan (TTGCM)

To understand the global structure and dynamics of Titan's thermosphere, Mueller-Wodarg et al. (2000) presented the first general circulation model for Titan's atmosphere above 600 km altitude. While this model, a collaborative project between University College London, the University of Arizona and Boston University, originally was based on the terrestrial thermosphere model of Fuller-Rowell and Rees (1980), it turned out that approximations frequently made for Earth are no longer valid on Titan, and ultimately a new model was developed from scratch. The Titan GCM predicted solar driven day-night temperature differences on Titan of up to 20 K which drive vigorous thermospheric dynamics. The extended nature of the thermosphere leads to effects such as continuous solar illumination also on the nightside at sufficiently polar latitudes. Subsequent studies showed that such winds would effectively redistribute constituents in Titan's thermosphere, particularly CH_4, causing large local time and hemispheric asymmetries in the CH_4 densities (Mueller-Wodarg and Yelle 2002; Mueller-Wodarg et al. 2003), as shown in Fig. 12. These calculations showed that dynamics and the distribution of CH_4 in Titan's thermosphere are intimately coupled. The first in-situ observations by the Cassini Ion Neutral Mass Spectrometer (INMS) showed that Titan's real thermosphere was more complex that suggested by the simple solar-driven calculations. Current developments of the model include adding the effects of more realistic dynamics at its lower boundary, which may importantly affect thermospheric dynamics. The model in its latest version is being constrained by densities observed by the INMS instrument.

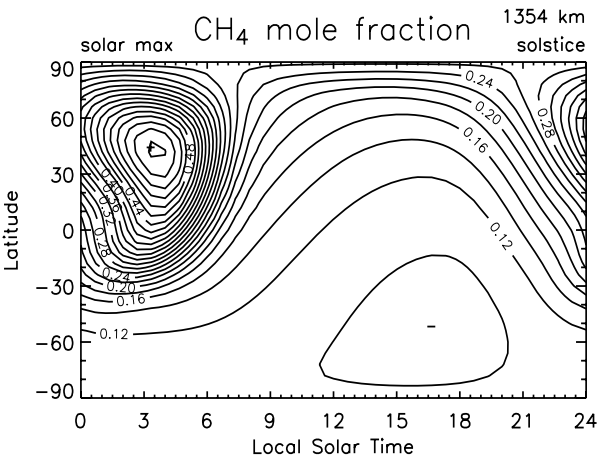

Fig. 12 CH_4 mole fractions near the 1×10^{-3} nbar pressure level for solstice at solar maximum, as calculated by the Titan TGCM. The average height of the pressure level is 1354 km

5 Modeling Frontiers and Problems

5.1 Lower to Upper Atmosphere Coupling

Properly addressing the coupling of the lower and upper atmospheres of planetary environments is a difficult modeling task. "Whole atmosphere" models are ultimately required to capture the physical processes (e.g., thermal, chemical, dynamical) throughout the entire atmosphere from the ground to the exobase. However, diffusion processes are much different above and below the homopause, requiring a method to be employed to bridge the transition between the homosphere and heterosphere regions. In addition, timescales for chemical and radiative processes vary greatly throughout the atmosphere, typically requiring small time-steps within finite-difference codes. Numerical stability (while utilizing longer time-steps) can be achieved in a number of ways; e.g., by employing implicit solvers and various numerical filters. Finally, exercising of multi-dimensional codes on multi-processor computers can also reduce the wall clock time for global simulations.

5.1.1 Separate but Coupled Model Frameworks vs. Whole Atmosphere Model Frameworks

Two approaches have been employed to date to capture the physics of the entire atmosphere (ground to exobase): (a) coupling of separate lower and upper atmosphere codes; and (b) single framework "whole atmosphere" model codes. Each approach has advantages and disadvantages. The coupling of separate codes permits the unique physical processes (and timescales) of the lower and upper atmospheres to be addressed separately within codes which can be optimized for this purpose. Molecular diffusion is one example for the upper atmosphere, for which an implicit (vertical) formulation permits a longer model time-step to be used. However, linking two separate models across an interface is not "seamless". By this we refer to the lack of an exact match of thermal and dynamical processes (e.g., solar heating, IR cooling, diffusion, numerical filtering) across this interface. Furthermore, both upward and downward coupling (i.e., constituent fluxes) is not easily activated across separate models. Whole atmosphere models obviate the need for an "artificial" boundary between 2-separate codes, while at the same time providing a continuous application of processes throughout the ground to exobase model domain. Small time-steps may be needed to accommodate disparate processes and their timescales throughout the model domain. Finally, whole atmosphere model simulations can be visualized from "top to bottom" with a single post-processor.

Examples of both modeling approaches are presented: (Sect. 5.1.2) the whole atmosphere model approach for Earth (NCAR WACCM), (Sect. 5.1.3) the coupled separate model approach for Mars (NASA MGCM and NCAR MTGCM), and (Sect. 5.1.4) the upward extended LMD-MGCM. The coupled model approach for Mars is a precursor to new Mars whole atmosphere models that are presently being developed and validated (see Table 1; see Sects. 4.2.3 and 5.1.4).

5.1.2 NCAR WACCM (Earth)

The WACCM model version 3 (WACCM3) is a state-of-the-art climate model developed at NCAR that extends from the Earth's surface to the lower thermosphere. This model is an outgrowth of three independent models developed separately across three divisions at NCAR. It combines the major features of these three independently developed models of the atmosphere, the Middle Atmosphere Community Climate Model (MACCM) (Boville 1995),

the chemical model MOZART (Brasseur et al. 1998) and the TIME-GCM (Roble 2000). This model is one of the few high-top general circulation models that include the Hamburg Model of the Neutral and Ionized Atmosphere (HAMMONIA) (Schmidt et al. 2006) and the extended Canadian Middle Atmosphere Model (CMAM) (Fomichev et al. 2002). These models have been used to study problems such as the solar influence on Earth's climate, constituent transport and trends in the middle atmosphere, the influence of the stratosphere on the tropospheric climate and the connection between climate change and polar mesospheric clouds. WACCM3 extends between the surface and the lower thermosphere near 140 km. But work is now progressing to move the upper boundary to 500–700 km by incorporating the aeronomy of the thermosphere and ionosphere from the TIME-GCM into an upward extended WACCM.

A number of studies are underway with this new model but one, Sassi et al. (2004), showed a coupling between El-Nino/Lanina ocean influences on the stratosphere/mesosphere region and another (Richter et al. 2008) showed the importance of gravity wave forcing on the basic structure of the upper atmosphere. Details of the model can be found on the web site http://www.cgd.ucar.edu/research/models/waccm.html.

5.1.3 NCAR Coupled MGCM-MTGCM (Mars)

The coupled NASA Ames MGCM and the NCAR MTGCM models constitute a numerical framework of 2-independent multi-dimensional codes linked across an interface at 1.32-microbars (∼60–80 km) in the Mars atmosphere (see Sect. 4.2.5). This coupled configuration permits both thermal and large scale dynamical processes to be linked across the lower and upper atmospheres of Mars (e.g., Bougher et al. 2004, 2006b). The 2-model treatment is designed to be a testbed for addressing coupling processes in advance of the development and validation of a comprehensive Mars "whole atmosphere" model framework (e.g. Sect. 4.2.3).

The coupled MGCM-MTGCM system itself has been used successfully to address/interpret an assortment of spacecraft observations, including Mars Global Surveyor, 2001 Mars Odyssey, and Mars Reconnaissance Orbiter thermosphere and/or ionosphere data sets (Bougher et al. 1999b, 2000, 2004, 2006b). For example, the recently discovered winter polar warming features of the Mars lower thermosphere (∼100–130 km) are found to vary greatly over the Mars seasons (e.g., Keating et al. 2003; Bougher et al. 2006b). Figure 13 illustrates coupled MGCM-MTGCM simulations for $Ls = 90$ (aphelion) and 270 (perihelion) conditions, demonstrating that the basic features of the Martian thermospheric winter polar warming are controlled by seasonal changes in the solar plus tidal forcing, the corresponding variations in the strength of the inter-hemispheric Hadley circulation, and the resulting changes in the magnitude of the adiabatic heating near the winter poles. Calculations of polar warming show that perihelion adiabatic heating can be highly variable from one Mars year to the next, and more than twice as strong as that for aphelion conditions (Bougher et al. 2006b; Bell et al. 2007). Finally, without the deep inter-hemispheric Hadley circulation made possible using these coupled lower and upper atmosphere simulations, winter polar warming features in the Mars thermosphere would not be reproduced at all (Bell et al. 2007).

Several studies are underway utilizing this coupled MGCM-MTGCM framework. For example, the role of interannual variations in horizontal and vertical dust distributions in affecting the thermospheric temperature and wind distributions is being investigated. Factors influencing the seasonal variation in the Mars mesopause heights and minimum temperatures are also being determined (McDunn et al. 2007, 2008).

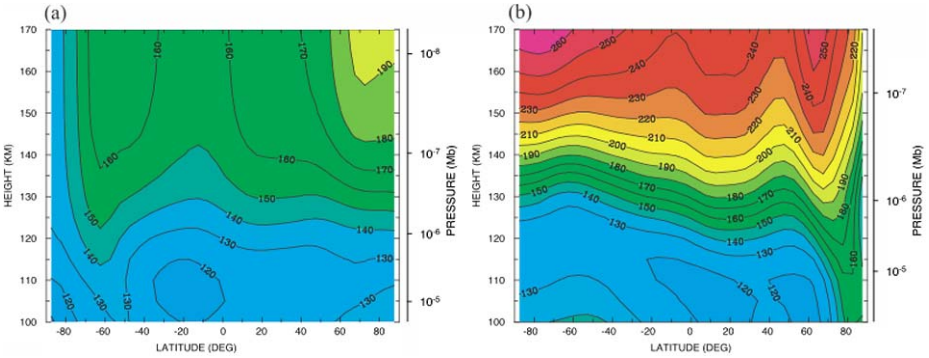

Fig. 13 MGCM-MTGCM zonal averaged temperature slices as a function of height and latitude: (**a**) $Ls = 90$ and (**b**) $Ls = 270$. Contour intervals are 10 K. Color shading is coordinated between these plots. From Bougher et al. (2006b)

5.1.4 LMD-MGCM (Mars)

The Mars LMD-GCM is based on the Terrestrial climate GCM of the Laboratoire de Meteorologie Dynamique (Sadourny and Laval 1984). It has been adapted by Hourdin et al. (1993) and Forget et al. (1999), who developed the first model covering the Martian atmosphere up to 80 km. The transport equations for the dynamics are directly taken from the LMD terrestrial GCM. They are based on a finite-difference formulation of the classical "primitive equations" of meteorology which are a simplified version of the general equations of fluids based on three main approximations: (1) the atmosphere is assumed to be a perfect gas; (2) it is supposed to remain vertically in hydrostatic equilibrium; and (3) the vertical dimension of the atmosphere is supposed to be much smaller than the radius of the planet (thin-layer approximation). The vertical discretization is based on σ-coordinates, where $\sigma = p/p_s$ is the pressure p at a given grid point normalized by its local value p_s at the surface of Mars (normalized pressure coordinates). The grid is chosen to have good coverage of the atmospheric boundary layer.

The energetics solved in the model includes the effects of suspended dust and CO_2 in the infrared in the Mars atmosphere. For the carbon dioxide, the thermal infrared and the near infrared absorption are solved using a NLTE approximation based on a parameterization of the heating and the cooling. Concerning the effect of dust, the radiative transfer of the solar radiation, including absorption and scattering, is modelled through a multi-stream approach. Then, the scattering of the thermal infrared outside the CO_2 15 μm band is modelled using a two-stream radiative transfer model. The CO_2 condensation-sublimation cycle is related to the thermal balance and is likely to a be source or sink of energy, mainly through the latent heat release associated with the change of state. This process is realistically included in the model and the different phases of carbon dioxide are managed consistently (in particular energy and mass conservation).

As mentioned above, the necessary discretization of time and space in the numerical model implies that mechanisms cannot be consistently modelled, because they occur at scales much below the lower limits of the model. They have to be added in an ad hoc way. The relevant processes that have been included near the surface of the planet at sub-grid scales are turbulent diffusion in the planetary boundary layer, convection, orography, and low-level drag.

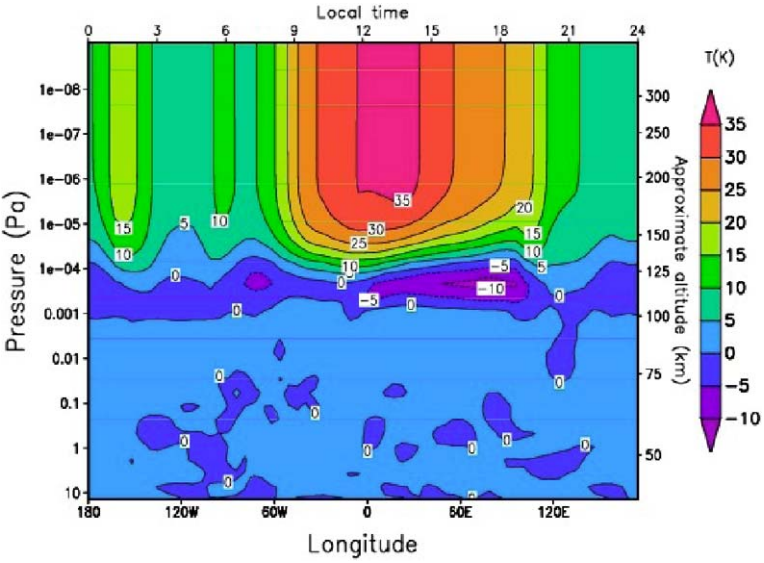

Fig. 14 Difference of temperatures between an LMD-GCM simulation without photochemistry and a simulation with photochemistry

The LMD-GCM extension to the thermosphere and the exosphere is a collaborative work with the University of Oxford and the Instituto de Astrofísicade Andalucía. The model has been successively extended from the ground up to a height of approximately 120 km (Angelats i Coll et al. 2003), 240 km (González-Galindo et al. 2004) and finally up to the exosphere (González-Galindo et al. 2007). The extension to the upper altitudes has been done in such a way that the processes that are important either in the mesosphere or in the thermosphere are taken into account.

In rarefied regions (thermospheres), each component of the neutral gas has an individual behaviour, which can be modelled using the Enskog approach, because this region is still collision dominated. We must distinguish horizontal from vertical dynamics, since the temporal and spatial scales are different. Temperature can be assumed to be the same for all the species, so a single equation for the temperature, which accounts for the thermal conductivity of the mean gas and the UV heating can be used. We do the same for the horizontal velocity, using a mean molecular viscosity. However, vertical diffusion is important in the upper atmosphere, and a multi-species Chapman-Enskog approach is used for multicomponent diffusion.

At upper altitudes, it is demonstrated that photochemistry becomes a very important feature of the atmospheric dynamics. A 1-D photochemical model using a complex photochemistry scheme, which includes the 12 major constituents of the C, O and H families, and accounts for 27 reactions between them has been developed and included in the LMD-GCM model. Figure 14 shows the impact that the photochemistry may have on the energy balance in the thermosphere. Temperature differences up to 35 K can be obtained above 200 km if some chemical processes are neglected.

The infrared processes related to CO_2, already mentioned above, are relevant processes for the mesosphere, and strongly NLTE in that region. Some approximation and parameterization has been done to include them, without increasing dramatically the computation time. The main heating source of the Martian thermosphere is the UV heating. In order to be able

to reproduce the thermal structure of the Martian upper atmosphere, which is critical for the hydrostatic equilibrium, as well as for dynamics, a parameterization has been included based on a full 1-D UV heating model. This full model includes the absorption by CO_2, O_2, atomic oxygen, H_2, H_2O, H_2O_2 and O_2 in the UV–visible range.

The GCM model has been used to build a database for Martian atmosphere (Lewis et al. 1999), which has become the ESA reference model for the atmosphere of Mars.

5.2 Thermosphere/Ionosphere to Exosphere Coupling

5.2.1 Previous Exosphere Modeling Approaches

As discussed in detail by Johnson et al. (2008), the hot coronae of atomic H, O and C have either been observed or postulated to exist at both Venus and Mars. The major reasons for interest in these hot populations are their importance in the long-term evolution of each atmosphere as well as the role they play in the general solar-wind interaction of each planet.

The history of Venus and Mars exospheric modeling approaches is contained in several early studies (e.g. Cravens et al. 1980; Nagy et al. 1981, 1990, 2001; Nagy and Cravens 1988; Kim et al. 1998; Hodges and Tinsley 1981, 1986; Hodges 2000). Both 1D models (based upon 2-stream calculations and Liouville's equation) plus multi-dimensional Monte Carlo particle trajectory models have been employed in these exospheric simulations. Recent 1D spherical Monte Carlo models have been constructed by Cipriani et al. (2007), extending the original work of Hodges (2000) to include hot O, C, CO_2 and CO. They also have examined more carefully the relative sources of dissociative recombination and atmospheric sputtering (Luhmann and Kozyra 1991) by O^+ pickup ions. Very recently Chaufray et al. (2007) published a study running a 3D Monte Carlo model for exospheric species, where they use the 1D ion profiles from the model of Krasnopolsky (2002) and as well as nightside ionosphere profiles obtained from Viking 1 measurements obtained from Zhang et al. (1990). They extrapolated these profiles around Mars for various SZAs and explored the 3D aspects of the related solar wind interaction processes.

5.2.2 Michigan Mars Exosphere Codes

In this section, the new approach of Valeille et al. (2007a, 2007b, 2008) is described which probes the effects of the 3D structure of the thermosphere on the exosphere. They use the results of a general circulation model, but perform 2D axisymmetric Direct Simulation Monte Carlo calculations for the SZA variation of the hot oxygen exosphere. The next major advance will be for the use of a 3D thermosphere-ionosphere model and a 3D exosphere model.

In order to merge the many local processes into a global picture, a model is needed, which can include these important processes on small spatial scales and which can diversify the different energy scales. The Michigan multi-species kinetic model is based on a technique called the Direct Simulation Monte Carlo (DSMC) method (Bird 1963, 1994). DSMC was developed to simulate the transition regime, where the mean free path of particles is too large for continuum hydrodynamics to be applicable. Individual particles are simulated as they move around within a grid, colliding with other particles and with solid objects (if any). Macroscopic properties, such as density, velocity and temperature are computed by appropriately averaging particle masses, locations, velocities, and internal energies. Momentum and energy exchanges with surfaces allow for chemical reactions and sputtering effects. Mass production can also be introduced as a boundary condition. DSMC is based on the "rarefied-gas" assumption that over a short time 'step' the molecular motion and

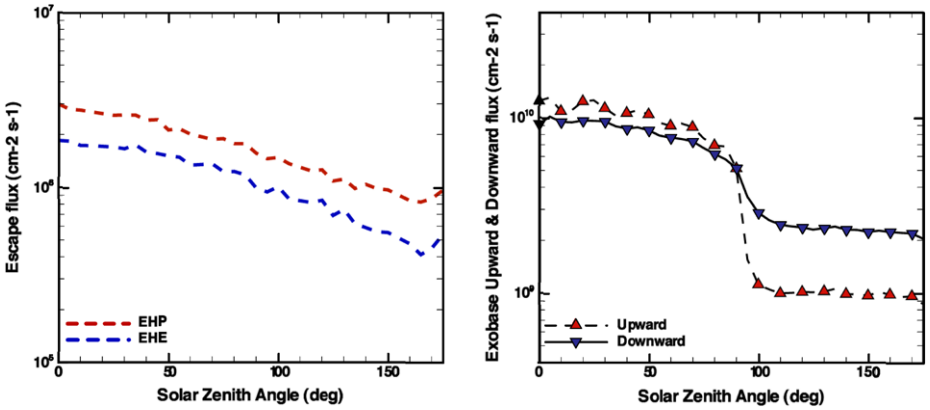

Fig. 15 Escape and upward and downward exobase fluxes of hot oxygen atoms for different solar conditions. Plotted on the *left* is the escape flux as a function of solar zenith angle for our new 2D axisymmetric Direct Simulation Monte Carlo model of the exosphere of Mars. In addition to the escape fluxes we are also calculating the return flux to the thermosphere and compare with what is normally assumed in thermosphere models. The separate upward and downward fluxes at the exobase are given in the plot on the *right*. *Left panel curves*: EHP (Equinox, High Solar Activity, Polar cut)—*top curve*; EHE (Equinox, High Solar Activity, Equatorial)—*bottom curve*

the intermolecular collisions are uncoupled and therefore can be calculated independently. Molecules are moved over the distances appropriate for this time step, followed by the calculation of a representative set of collisions. The time step is small compared to the mean collision time, and the results are independent of its actual value.

The Michigan DSMC code was developed with the dusty-gas comet coma as the first science application (Tenishev et al. 2008) improving in a number of fundamental and technical ways over the original comet DSMC of Combi (1996). It was also developed as a general-purpose gas kinetic solver and tested against a number of standard aerodynamical gas kinetic problems (Tenishev and Combi 2003a, 2003b) as well as comets. The code has been applied both to Mars' exosphere (Valeille et al. 2007a, 2007b, 2008) and plumes of Enceladus (Tenishev et al. 2007, 2008).

Valeille et al. (2007a, 2007b, 2008) have applied DSMC to the hot atomic oxygen corona of Mars, using the 3D MTGCM of Bougher et al. (2006b) (see Sect. 4.2.5) to understand the overall day-night structure of the exosphere as well as to explore day-night, local time, meridian, latitudinal, seasonal and solar activity variations. The goals are to understand the range and limits on the escape rate, exosphere distribution, as well as the return fluxes of exospheric O to the thermosphere.

A set of 2D axisymmetric DSMC models have been run with coordinates of radius and SZA for a variety of upper thermosphere conditions taken from the 3D MTGCM: for quiet and active sun, for equinox conditions, for solstice conditions (both at aphelion and perihelion), and for thermosphere distributions around the equator and along the polar noon-midnight meridian. The escape rates and exobase upward and downward fluxes as a function of SZA for an equinox geometry at solar high (active) and solar low (quiet) conditions are shown in Fig. 15. In addition, Fig. 16 shows the O density distribution in the corona for the solar maximum and solar minimum models for the equinox geometry. Finally, Fig. 17 shows the O atom escape rates for solar maximum and minimum conditions for the new results by Valeille et al. (2007a, 2007b, 2008) compared with published values from the literature.

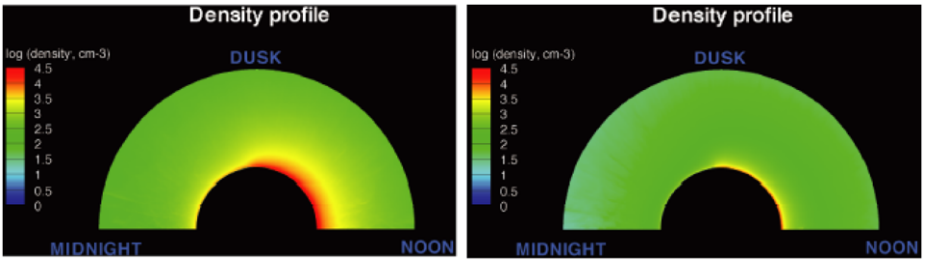

Fig. 16 Hot oxygen density for different solar conditions. Shown is a false *color contour plot* of the hot oxygen atom exospheric density for (**a**) solar active and (**b**) solar quiet conditions of the MTGCM model. Using the same *color-table* highlights the differences of the exosphere for active and quiet solar conditions

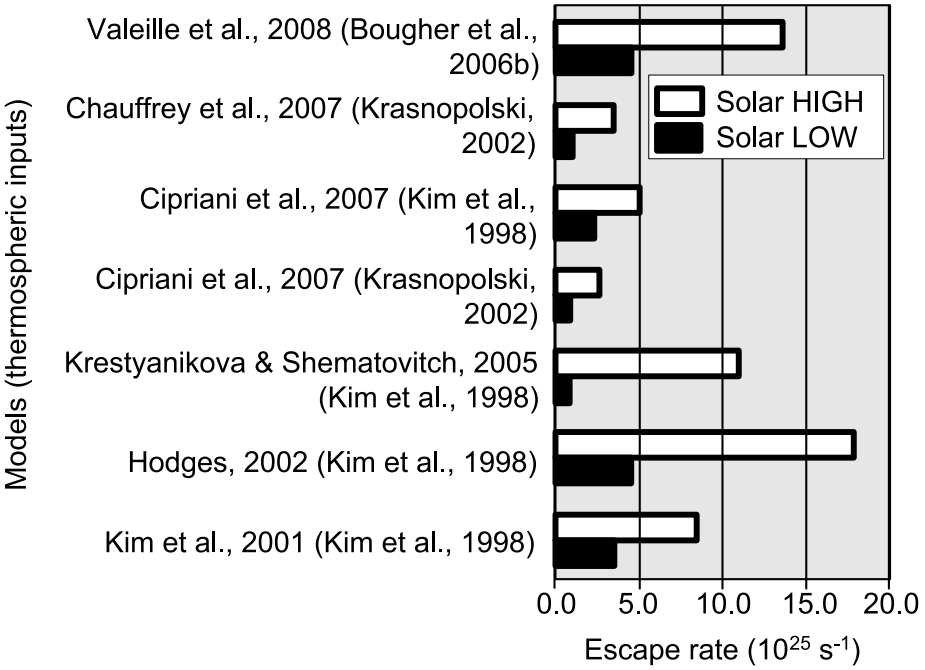

Fig. 17 Comparison of O atom escape rates from various models (from Valeille et al. 2008). Shown are the solar minimum and solar maximum escape rates from several models with the thermosphere conditions used, given in parentheses. Kim et al. (1998) is corrected by a factor of 6.5 according to Nagy et al. (2001). The Valeille et al. (2008) escape rate, averaged over the solar cycle and Mars seasons, is $\sim 1.0 \times 10^{26}$ s^{-1}. Detailed Mars orbiter photochemical escape measurements are needed to validate these models

The general structure of the exosphere and escape fluxes is similar from time to time, but the actual values of the escape rates in the extreme model cases can range over nearly a factor of 50 when comparing conditions from solar minimum to maximum, and from Mars perihelion and aphelion solstices with the equinoxes that are between the two extremes. These results clearly imply that the next step in modeling Mars' exosphere needs to be done with a 3D exosphere model using a realistic 3D thermosphere for its base assumption.

References

N. Achilleos, S. Miller, J. Tennyson, A. Aylward, I. Mueller-Wodarg, D. Rees, J. Geophys. Res. **103**, 20089–20112 (1998). doi:10.1029/98JE00947

N. Achilleos, S. Miller, R. Prangé, G. Millward, M.K. Dougherty, N.J. Phys. **3** (2001). doi:10.1088/1367-2630/3/1/303

M. Angelats i Coll, F. Forget, M.A. López-Valverde, P.L. Read, S.R. Lewis, J. Geophys. Res. **109**, 1011 (2003). doi:10.1029/2003JE002163

J.M. Bell, The dynamics of the upper atmospheres of Mars and Titan. Ph.D Thesis, University of Michigan (2008)

J.M. Bell, S.W. Bougher, V. De LaHaye, J.H. Waite Jr., A. Ridley, Eos Trans. Am. Geophys. Union **87**(Jt. Assem. Suppl.) (2006), abstract U52A-06

J.M. Bell, S.W. Bougher, J.R. Murphy, J. Geophys. Res. **112**, E12002 (2007). doi:10/1029/2006JE002856

J.-L. Bertaux et al., Science **307**, 566–569 (2005)

G.A. Bird, Phys. Fluids **6**, 1518–1519 (1963)

G.A. Bird, *Molecular Gas Dynamics and the Direct Simulations of Gas Flows* (Clarendon, Oxford, 1994)

V. Boqueho, P.-L. Blelly, J. Geophys. Res. **110**, A01313 (2005). doi:10.1029/2004JA010414

S.W. Bougher et al., Icarus **68**, 284–312 (1986)

S.W. Bougher, R.E. Dickinson, E.C. Ridley, R.G. Roble, Icarus **73**, 545–573 (1988)

S.W. Bougher, J.C. Gerard, A.I.F. Stewart, C.G. Fesen, J. Geophys. Res. **95**, 6271–6284 (1990)

S.W. Bougher, W.J. Borucki, J. Geophys. Res. **99**, 3759–3776 (1994)

S.W. Bougher, D.M. Hunten, R.G. Roble, J. Geophys. Res. **99**, 14609–14622 (1994)

S.W. Bougher, M.J. Alexander, H.G. Mayr, in *Venus II*, ed. by S.W. Bougher, D.M. Hunten, R.J. Philips (University of Arizona Press, Tucson, 1997), pp. 259–292

S.W. Bougher, S. Engel, R.G. Roble, B. Foster, J. Geophys. Res. **104**, 16591–16611 (1999a)

S.W. Bougher et al., Adv. Space Res. **23**(11), 1887–1897 (1999b)

S.W. Bougher, S. Engel, R.G. Roble, B. Foster, J. Geophys. Res. **105**, 17,669–17,689 (2000)

S.W. Bougher, R.G. Roble, T.J. Fuller-Rowell, in *Atmospheres in the Solar System: Comparative Aeronomy*, ed. by M. Mendillo, A. Nagy, H. Waite. Geophysical Monograph, vol. 130 (American Geophysical Union, Washington, 2002), pp. 261–288

S.W. Bougher, S. Engel, D.P. Hinson, J.R. Murphy, J. Geophys. Res. **109**, E03010 (2004). doi:10.1029/2003JE002154

S.W. Bougher, J.H. Waite, T. Majeed, G.R. Gladstone, J. Geophys. Res. **110**, E04008 (2005). doi:10.1029/2003JE002230

S.W. Bougher, S. Rafkin, P. Drossart, Planet. Space Sci. **54**, 1371–1380 (2006a)

S.W. Bougher, J.M. Bell, J.R. Murphy, M.A. López-Valverde, P.G. Withers, Geophys. Res. Lett. **33**, L02203 (2006b). doi:10.1029/2005GL024059

S.W. Bougher, A. Brecht, C. Parkinson, S. Rafkin, B. Foster, 37th COSPAR Scientific Assembly 2008, C32-0003-08 Abstract (2008)

B.A. Boville, J. Geophys. Res. **100**, 9017–9039 (1995)

G.P. Brasseur et al., J. Geophys. Res. **103**, 28265–28290 (1998)

A. Brecht, S.W. Bougher, S. Rafkin, B. Foster, Eos Trans. Am. Geophys. Union **88**(52), (Fall Meeting Suppl.) (2007), abstract P33B-1299

J.Y. Chaufray et al., J. Geophys. Res. **112**, E09009 (2007). doi:10.1029/2007JE002915

R.H. Chen, A.F. Nagy, J. Geophys. Res. **83**, 1133–1140 (1978)

R.H. Chen, T.E. Cravens, A.F. Nagy, J. Geophys. Res. **83**, 3871–3876 (1978)

F. Cipriani, F. Leblanc, J.J. Berthelier, J. Geophys. Res. **112**, D07001 (2007). doi:10.1029/2006JE002818

M.R. Combi, Icarus **123**, 207–226 (1996)

T.E. Cravens, T.I. Gombosi, A.F. Nagy, Nature **283**, 178–180 (1980)

T.E. Cravens, A.J. Kliore, J.U. Kozyra, A.F. Nagy, J. Geophys. Res. **86**, 11,323–11,329 (1981)

V. DeLa Haye, Coronal formation and heating efficiencies in Titan's upper atmosphere: Construction of a coupled ion, neutral and thermal structure model to interpret the first INMS Cassini data. Ph.D. Thesis, University of Michigan, Ann Arbor (2005)

Y. Deng, A.D. Richmond, A.J. Ridley, H. Liu, Geophys. Res. Lett. **35**, L01104 (2008). doi:10.1029/2007GL032182

A.L. Dobbin, A.D. Aylward, M.J. Harris, J. Geophys. Res. **111**, A07314 (2006). doi:10.1029/2005JA011543

A. Eviatar, A.D. Barbosa, J. Geophys. Res. **89**, 7393–7398 (1984)

P.R. Field et al., J. Atmos. Sol. Terr. Phys. **60**, 523–543 (1998)

M.O. Fillingim et al., Geophys. Res. Lett. **34**, L12101 (2007). doi:10.1029/2007GL029986

V.I. Fomichev et al., J. Geophys. Res. **107** (2002). doi:1029/2001JD000479

J.M. Forbes, F.G. Lemoine, S.L. Bruinsma, M.D. Smith, X. Zhang, Geophys. Res. Lett. **35**, L01201 (2008). doi:10.1029/2007GL031904
F. Forget et al., J. Geophys. Res. **104**, 24155–24176 (1999). doi:10.1029/1999JE001025
J.L. Fox, Icarus **51**, 248–260 (1982)
J.L. Fox, Planet. Space Sci. **36**, 37–46 (1988)
J.L. Fox, in *Venus and Mars: Atmospheres, Ionospheres and Solar Wind Interaction*, ed. by J.G. Luhmann, M. Tatrallyay, R. Pepin. Geophysical Monograph, vol. 66 (AGU Press, Washington, 1992), pp. 191–222
J.L. Fox, J. Geophys. Res. **109**, A11310 (2004). doi:10.1029/2004JA010380
J.L. Fox, A. Dalgarno, J. Geophys. Res. **84**, 7315–7333 (1979)
J.L. Fox, A. Dalgarno, J. Geophys. Res. **86**, 629–639 (1981)
J.L. Fox, K.Y. Sung, J. Geophys. Res. **106**(A10), 21305–21336 (2001)
J.L. Fox, K.E. Yeager, J. Geophys. Res. **111** (2006). doi:10.1029/2006JA011697
J.L. Fox, P. Zhou, S.W. Bougher, Adv. Space Res. **17**, (11)203–(11)218 (1995)
T.J. Fuller-Rowell, J. Geophys. Res. **103**, 3951–3956 (1998)
T.J. Fuller-Rowell, D. Rees, J. Atmos. Sci. **37**, 2545–2567 (1980)
T.J. Fuller-Rowell, D. Rees, Planet. Space Sci. **10**, 1209–1222 (1983)
T.J. Fuller-Rowell, D. Rees, S. Quegan, R.J. Moffett, G.J. Bailey, J. Geophys. Res. **92**, 7744–7748 (1987)
T.J. Fuller-Rowell et al., in *STEP Handbook on Ionospheric Models*, ed. by R.W. Schunk (Utah State University, Logan, 1996)
T.J. Fuller-Rowell, G.H. Millward, A.D. Richmond, M.V. Codrescu, J. Atmos, Sol.-Terr. Phys. **64**, 1383–1391 (2002)
F. González-Galindo, M.A. López-Valverde, M. Angelats i Coll, F. Forget, J. Geophys. Res. **110**, 9005 (2004). doi:10.1029/2004JE002312
F. González-Galindo, F. Forget, M.A. López-Valverde, M. Angelats i Coll, S.W. Bougher, LPI Contributions **1353**, 3099 (2007)
R.M. Haberle et al., J. Geophys. Res. **104**(E4), 8957–8974 (1999)
W.B. Hanson, S. Sanatani, D.R. Zuccaro, J. Geophys. Res. **82**, 4351–4367 (1977)
M.J. Harris, A new coupled middle atmosphere and thermosphere general circulation model: Studies of dynamic, energetic and photochemical coupling in the middle and upper atmosphere. Ph.D Thesis, University College London (2001)
R.R. Hodges, J. Geophys. Res. **105**, 6971–6981 (2000)
R.R. Hodges, Geophys. Res. Lett. **29**(3), 1038 (2002). doi:10.1029/2001GL013852
R.R. Hodges, B.A. Tinsley, J. Geophys. Res. **86**, 7649–7656 (1981)
R.R. Hodges, B.A. Tinsley, J. Geophys. Res. **91**, 13649–13659 (1986)
F. Hourdin, P. Le Van, F. Forget, O. Talagrand, Meteorological variability and the annual pressure cycle on Mars. J. Atmos. Sci. **50**, 3625–3640 (1993)
W.B. Hubbard et al., Astron. Astrophys. **269**, 541–563 (1993)
R.E. Johnson et al., Space Sci. Rev. (2008, this issue)
W.T. Kasprzak et al., in *Venus II*, ed. by S.W. Bougher, D.M. Hunten, R.J. Philips (University of Arizona Press, Tucson, 1997), pp. 225–257
G.M. Keating, N.C. Hsu, Geophys. Res. Letts. **20**, 2751–2754 (1993)
G.M. Keating, J.Y. Nicholson III, L.R. Lake, J. Geophys. Res. **85**, 7941–7956 (1980)
G.M. Keating et al., Science **279**, 1672–1676 (1998)
G.M. Keating et al., Brief review on the results obtained with the MGS and Mars Odyssey 2001 Accelerometer Experiments. International Workshop: Mars Atmosphere Modeling and Observations, Inst. de Astrofis. de Andalucia, Granada, Spain, paper (2003)
D. Kella, L. Vejby-Christenson, P.J. Johnson, H.B. Pedersen, L.H. Andersen, Science **276**, 1530–1533 (1997)
J.T. Khiel et al., J. Clim. **11**, 1131–1149 (1998)
J. Kim, A.F. Nagy, T.E. Cravens, A.J. Kliore, J. Geophys. Res. **94**, 11,997–12,002 (1989)
J. Kim, A.F. Nagy, J.L. Fox, T.E. Cravens, J. Geophys. Res. **103**(12), 29,339–29,342 (1998)
Y.H. Kim, S. Son, Y. Yi, J. Kim, J. Kor. Ast. Soc. **34**, 25–29 (2001)
A.J. Kliore, G.S. Levy, D.L. Cain, G. Fjeldbo, S.I. Rasool, Science **205**, 99–102 (1967)
V.A. Krasnopolsky, *Photochemistry of the Atmospheres of Mars and Venus* (Springer, Berlin, 1982)
V.A. Krasnopolsky, J. Geophys. Res. **107**(E12), 5128 (2002). doi:10.1029/2001JE001809
M.A. Krestyanikova, V.I. Shematovitch, Sol. Syst. Res. **39**, 22–32 (2005)
S. Kumar, D.M. Hunten, J. Geophys. Res. **79**, 2529–2532 (1974)
S.R. Lewis et al., J. Geophys. Res. **104**, 24,177–24,194 (1999)
H.-L. Liu, R.G. Roble, J. Geophys. Res. **107**(D23), 4695 (2002). doi:10.1029/2001JD001533
H.-L. Liu, R.G. Roble, Geophys. Res. Lett. **32**, L13804 (2005). doi:10.1029/2005GL022939
K. Lodders, B. Fegley Jr., *The Planetary Scientists Companion* (Oxford University Press, New York, 1998)

M.A. López-Valverde, D.P. Edwards, M. López-Puertas, C. Roldán, J. Geophys. Res. **103**(E7), 16,799–16,812 (1998)
J.G. Luhmann, J.U. Kozyra, J. Geophys. Res. **96**, 5457–5467 (1991)
Y. Ma, A.F. Nagy, I.V. Sokolov, K.C. Hansen, J. Geophys. Res. **109**, A07211 (2004). doi:10.1029/2003JA010367
T. Majeed, J.H. Waite Jr., S.W. Bougher, G.R. Gladstone, J. Geophys. Res. **110**, E12007 (2005). doi:10.1029/2004JE002351
T. Majeed, J.H. Waite Jr., S.W. Bougher, G.R. Gladstone, J. Geophys. Res. (2008, submitted)
C.R. Martinis, J.K. Wilson, M.J. Mendillo, J. Geophys. Res. **108**(A10), 1383 (2003). doi:10.1029/2003/JA009973
E. Mazarico, M.T. Zuber, F.G. Lemoine, D.E. Smith, Eos Trans. Am. Geophys. Union **88**(Fall Meeting Suppl.) (2007), abstract P32A-04
T.L. McDunn et al., The 7th International Conference on Mars, Pasadena, CA (2007), abstract XX
T.L. McDunn et al., AGU Chapman conference on the solar wind interaction with Mars. San Diego (2008), abstract A-07
M.B. McElroy, Astrophys. J. **150**, 1125–1138 (1967)
M.B. McElroy, J. Geophys. Res. **73**, 1513–1521 (1968a)
M.B. McElroy, J. Atmos. Sci. **25**, 574–577 (1968b)
M.B. McElroy, J. Geophys. Res. **74**, 29–42 (1969)
M.B. McElroy et al., Science **194**, 1295–1298 (1976)
M.B. McElroy, T.Y. Kong, Y.L. Yung, A.O. Nier, Science **194**, 1295–1298 (1976)
G.H. Millward, R.J. Moffett, S. Quegan, T.J. Fuller-Rowell, in *STEP Handbook on Ionospheric Models*, ed. by R.W. Schunk (Utah State University, Logan, 1996a)
G.H. Millward, H. Rishbeth, R.J. Moffett, S. Quegan, T.J. Fuller-Rowell, J. Geophys. Res. **101**, 5149–5156 (1996b)
G.H. Millward et al., J. Geophys. Res. **106**(A11), 24,733–24,744 (2001)
G.H. Millward, S. Miller, A.D. Aylward, I.C.F. Mueller-Wodarg, N. Achilleos, in *Comparative Atmospheres in the Solar System*, ed. by M. Mendillo, A. Nagy, J.H. Waite (American Geophysical Union, Washington, 2002a), pp. 289–298
G.H. Millward, S. Miller, T. Stallard, A.D. Aylward, Icarus **160**, 95–107 (2002b)
G.H. Millward, S. Miller, T. Stallard, N. Achilleos, A.D. Aylward, Icarus **173**, 200–211 (2005)
L. Moore, M. Mendillo, Geophys. Res. Lett. **34**, L12202 (2007). doi:10.1029/2007GL029381
L. Moore et al., Geophys. Res. Lett. **33**, L22202 (2006). doi:10.1029/2006GL027375
L.E. Moore, M. Mendillo, I.C.F. Mueller-Wodarg, D.L. Murr, Icarus **172**, 503–52 (2004)
I.C.F. Mueller-Wodarg, R.V. Yelle, Geophys. Res. Lett. **29** (2002). doi:10.1029/2002GL016100
I.C.F. Mueller-Wodarg, R.V. Yelle, M. Mendillo, L.A. Young, A.D. Aylward, J. Geophys. Res. **105**, 20833–20856 (2000)
I.C.F. Mueller-Wodarg, R.V. Yelle, M. Mendillo, A.D. Aylward, J. Geophys. Res. **108**(A12), 1453 (2003). doi:10.1029/2003JA010054
I.C.F. Mueller-Wodarg, M. Mendillo, R.V. Yelle, A.D. Aylward, Icarus **180**, 147–160 (2006)
I.C.F. Mueller-Wodarg et al., Space Sci. Rev. (2008, this issue)
A.F. Nagy, T.E. Cravens, Geophys. Res. Lett. **15**, 433–435 (1988)
A.F. Nagy, J. Kim, T.E. Cravens, Ann. Geophys. **8**, 251–256 (1990)
A.F. Nagy, T.E. Cravens, S.G. Smith, H.A. Taylor, H.C. Brinton, J. Geophys. Res. **85**, 7795–7801 (1980)
A.F. Nagy, T.E. Cravens, J.H. Yee, A.I.F. Stewart, Geophys. Res. Lett. **8**, 629–632 (1981)
A.F. Nagy, M.W. Liemohn, J.L. Fox, J. Kim, J. Geophys. Res. **106**(10), 21,565–21,568 (2001)
A.F. Nagy et al., J. Geophys. Res. **111**, A06310 (2006). doi:10.1029/2005JA011519
A.O. Nier, M.B. McElroy, Science **194**, 1298–1300 (1976)
L. Qian, S.C. Solomon, R.G. Roble, T.J. Kane, Geophys. Res. Lett. **33**, L23705 (2006). doi:10.1029/2006GL027185
L. Qian, S.C. Solomon, R.G. Roble, T.J. Kane, Geophys. Res. Lett. **35**, L07811 (2008). doi:10.1029/2007GL033156
S. Quegan et al., J. Atmos. Terr. Phys. **44**, 619–640 (1982)
S. Rafkin, A. Stern, S. Bougher, A. Brecht, Venus Express Science team meeting. Abstract, Thuile, Italy, March 18–24 (2007)
A.D. Richmond, E.C. Ridley, R.G. Roble, Geophys. Res. Lett. **19**, 601–604 (1992)
J.H. Richter, F. Sassi, R.R. Garcia, K. Matthes, C.A. Fischer, *J. Geophys. Res.* (2008, in press)
A.J. Ridley, Y. Deng, G. Toth, J. Atmos. Sol. Terr. Phys. **68**, 839 (2006)
H. Rishbeth, I.C.F. Mueller-Wodarg, Ann. Geophys. **17**, 794–805 (1999)
H. Rishbeth et al., Ann. Geophysicae **18**, 945–956 (2000a)
H. Rishbeth, R.V. Yelle, M. Mendillo, Planet. Space. Sci. **48**, 51–58 (2000b)

R.G. Roble, in *The Upper Mesosphere Lower Thermosphere: A Review of Experiment and Theory*, ed. by R.M. Johnson, T.L. Killeen. Geophysical Monograph, vol. 87 (American Geophysical Union, 1995), p. 1
R.G. Roble, in *Atmospheric Science Across the Stratopause*. Geophysical Monograph, vol. 123 (American Geophysical Union, 2000), pp. 53–67
R.G. Roble, R.E. Dickinson, Geophys. Res. Lett. **16**, 1441–1444 (1989)
R.G. Roble, E.C. Ridley, Geophys. Res. Lett. **21**, 417–420 (1994)
R.G. Roble, E.C. Ridely, R.E. Dickinson, J. Geophys. Res. **92**, 8745–8758 (1987)
C. Roldan, M.A. Lopez-Valverde, M. Lopez-Puertas, D.P. Edwards, Icarus **147**, 11–25 (2000)
R. Sadourny, K. Laval, in *New Perspectives in Climate Modeling*, ed. by A. Berger, C. Nicolis (Elsevier, Amsterdam, 1984), pp. 173–197
F. Sassi, D. Kinneson, B.A. Boville, R.R. Garcia, R.G. Roble, J. Geophys. Res. **109**, D17108 (2004). doi:10.1029/2003JD004434
H.G. Schmidt et al., J. Climate **19** (2006). doi:10.1175/JCLI3829.1
G. Schubert et al., in *Exploring Venus as a Terrestrial Planet*. Geophysical Monograph, vol. 176 (American Geophysical Union, 2007), pp. 101–120
R.W. Schunk, A.F. Nagy, *Ionospheres: Physics, Plasma Physics and Chemistry*. Cambridge Atmospheric and Space Science Series (Cambridge University Press, Cambridge, 2000)
R. Shimazaki, M. Shimizu, Rep. Ionos. Space Res. Jpn. **24**, 80–98 (1970)
H. Shinagawa, T.E. Cravens, J. Geophys. Res. **93**, 11,263–11,277 (1988)
H. Shinagawa, T.E. Cravens, J. Geophys. Res. **94**, 6506–6516 (1989)
C.G.A. Smith, S. Miller, A.D. Aylward, Ann. Geophys. **23**, 1943–1947 (2005)
R.W. Stewart, J. Atmos. Sci. **25**, 578–582 (1968)
R.W. Stewart, J. Atmos. Sci. **28**, 1069–1073 (1971)
D.F. Strobel, in *Atmospheres in the Solar System: Comparative Aeronomy*, ed. by M. Mendillo, A. Nagy, H. Waite. Geophysical Monograph, vol. 130 (American Geophysical Union, Washington, 2002), pp. 7–22
V.T. Tenishev, M.R. Combi, AIAA Paper 2003-3776 (2003a)
V.T. Tenishev, M.R. Combi, RGD, 23rd Int. Symp. 663, 696 (2003b)
V.T. Tenishev, M. Combi, H. Waite, Eos Trans. Am. Geophys. Union **88**(23) (Jt. Assem. Suppl.) (2007), abstract P43A-02
V.T. Tenishev, M.R. Combi, B. Davidsson, Astrophys. J. (2008, in press)
R.H. Tolson et al., J. Spacecr. Rockets **44**(6), 1172–1179 (2007)
A. Valeille, V. Tenishev, S.W. Bougher, M.R. Combi, A.F. Nagy, Eos Trans. Am. Geophys. Union **88**(23) (Jt. Assem. Suppl.) (2007a), abstract SA31B-02
A. Valeille, V. Tenishev, S.W. Bougher, M.R. Combi, A.F. Nagy, B. A. A. S. **39**, #24.01 (2007b)
A. Valeille, M.R. Combi, V.T. Tenishev, S.W. Bougher, A.F. Nagy, Icarus (2008, submitted)
U. von Zahn et al., J. Geophys. Res. **85**, 7829–7840 (1980)
J.H. Waite et al., Science **308**, 982–986 (2005)
O. Witasse et al., Space Sci. Rev. (2008, this issue)
P.G. Withers, Geophys. Res. Letts. **33**, L02201 (2006). doi:10.1029/2005GL024447
R.V. Yelle, S. Miller, in *Jupiter: The Planet, Satellites, and Magnetosphere*, ed. by F. Bagenal, T.E. Dowling, W.B. McKinnon (Cambridge Univ. Press, New York, 2004), pp. 185–218
M.H.G. Zhang, J.G. Luhmann, A.J. Kliore, J. Kim, J. Geophys. Res. **95**, 14829–14839 (1990)
S. Zhang, S.W. Bougher, M.J. Alexander, J. Geophys. Res. **101**, 23195–23205 (1996)